PU.1 and MYC transcriptional network defines synergistic drug responses to KIT and LSD1 inhibition in acute myeloid leukemia

Brittany M. Smith[1], Jake VanCampen[1], Garth L. Kong[1], William Yashar[1], Wesley Horton[1], Daniel J. Coleman[1], Joseph Estabrook[1,2], Theresa A. Lusardi[2], Brain J. Druker[1,3] Julia E. Maxson[1,3], Theodore P. Braun[1,3*]

Knight Cancer Institute[1], Cancer Early Detection Advanced Research Center[2], Division of Hematology & Medical Oncology[3], Oregon Health & Science University, Portland, Oregon, 97239, USA.

CORRESPONDENCE:
Theodore P. Braun
Knight Cancer Institute
3181 SW Sam Jackson Pk. Rd., KR-HEM
Portland, Oregon, 97239
braunt@ohsu.edu

Abstract

Activating mutations in the KIT tyrosine receptor kinase confer an adverse prognosis for patients with acute myeloid leukemia (AML). Successful treatment options are limited, as kinase inhibition monotherapy for AML is often followed by rapid drug resistance. Here we demonstrate that combined KIT and LSD1 inhibition causes increased cytotoxicity and may mitigate the propensity for relapse with kinase inhibition. This combination suppresses MYC at both the transcript and protein level to drive cell cycle exit and cell death. This decreased MYC transcript expression results from a loss of PU.1 binding at a downstream MYC enhancer leading to decreased acetylation at the MYC enhancer and promoter. Additionally, the drug combination inactivates PI3K/AKT/GSK3 signaling to decrease MYC protein stability. Within 24 hours, KIT-mutant AML cells adapt to KIT inhibitor monotherapy by restoring PI3K/AKT activity. However, with the addition of a LSD1 inhibitor, PI3K/AKT activity cannot be restored. Taken together, KIT and LSD1 inhibition cooperatively target MYC activity through altered transcription and modulation of signaling to drive a lasting response. In addition, we validate MYC suppression as a mechanism of synergy between KIT and LSD1 inhibition in KIT-mutant AML patient samples. Collectively, this work provides rational for a clinical trial to assess the efficacy of KIT and LSD1 inhibition in patients with KIT-mutant AML.

Introduction

Acute myeloid leukemia (AML) results from the acquisition of two or more oncogenic mutations leading to proliferative advantage and hematopoietic differentiation block[1]. Kinase mutations frequently provide this proliferative advantage, but are insufficient to produce AML in isolation[1]. These mutations occur later in leukemogenesis, and are preceded by other genetic abnormalities[2–4]. In contrast, mutations altering transcriptional or epigenetic regulatory proteins occur early in the disease course[4,5]. The treatment AML with kinase inhibitors has limited clinical efficacy due to short-lived responses and the inevitable development of drug resistance[6–8]. Approaches to augment the efficacy of kinase inhibition by co-targeting of the leukemic epigenome represents a promising approach to obtain deeper and longer responses[9].

Epigenetic drugs have so far shown limited efficacy as monotherapy, with few patients demonstrating profound changes in disease volume[10–12]. However, there is promising evidence showing increased efficacy when epigenetic drugs and kinase inhibitors are used in combination. Previously, we have showed that dual inhibition of JAK/STAT and an epigenetic regulator, lysine-specific demethylase 1 (LSD1) is an effective therapeutic strategy for CEBPA/CSF3R mutant AML[13]. Inhibition of LSD1 restored differentiation-associated enhancer activity, further potentiating the action of JAK/STAT inhibitors in vitro and in vivo[13]. Core binding factor (CBF) translocated AML shows a high degree of epigenetic similarity to CEBPA mutant AML resulting in a differentiation block, yet is associated with different signaling mutations[14,15]. KIT mutations are the most common signaling mutation in CBF AML and drive proliferation via downstream JAK/STAT and MAPK pathway activation[16–18]. CBF AML alone is favorable risk, however, the presence of KIT mutations is associated with an increased risk of relapse[16,19]. Avapritinib (BLU-285) is a KIT inhibitor that is currently approved by the US Food and Drug Administration (FDA) for advanced systemic mastocytosis and gastrointestinal stromal tumor (GIST), both of which have activating KIT mutations (NCT00782067, NCT02508532). Given the short-lived responses to therapeutic inhibition of other kinases in AML, avapritinib monotherapy is unlikely to produce durable responses in KIT-mutant AML. However, given the efficacy of kinase plus LSD1 inhibition other AML subtypes, this approach warrants investigation for the treatment of KIT mutant AML.

Here, we demonstrate that LSD1 inhibition potentiates the activity of the KIT inhibitor, avapritinib, in leukemia cell lines and primary patient samples. This synergistic cytotoxicity is driven by perturbation in the MYC and PU.1 transcription factor networks, resulting in decreased expression of proliferation associated genes. These mechanistic findings provide a basis for extending this dual therapeutic strategy into other molecularly defined subtypes of AML. Additionally, we identified key biomarkers to assess drug efficacy in KIT mutant AML.

Materials and Methods

Cell Lines

Kasumi-1 (ATCC), CMK (DSMZ) and MOLM-13 (DSMZ) cells were cultured in RPMI (Gibco) supplemented with 20% fetal calf serum (FCS, HyClone), 2 mM GlutaMAX (Gibco), 100 units/mL Penicillin, and 100 ug/mL Streptomycin (Gibco). K562 (ATCC) cells were cultured in RPMI supplemented with 10% FBS. SNKO-1 cells were obtained from DSMZ and cultured in RPMI with 10% FSB and 10 ng/ml GM-CSF (PeproTech). EOL-1 cells were obtained from DSMZ and cultured in RPMI with 10% FBS. Patient samples were cultured in RPMI with 10% FBS and 50% HS-5 conditioned media (ATCC) or SFEMII supplemented with 1x StemSpan CD34+ Expansion Media and 1 uM UM729 (StemCell Technologies). All cells were cultured at 5% CO_2 and 37°C. Cell lines were tested monthly for mycoplasma contamination.

Patient Samples

All patients gave informed consent to participate in this study, which had the approval and guidance of the institutional review boards at Oregon Health & Science University (OHSU), University of Utah, University of Texas Medical Center (UT Southwestern), Stanford University, University of Miami, University of Colorado, University of Florida, National Institutes of Health (NIH), Fox Chase Cancer Center and University of Kansas (KUMC). Samples were sent to the coordinating center (OHSU; IRB#9570; #4422; NCT01728402) where they were coded and processed. Mononuclear cells were isolated by Ficoll gradient centrifugation from freshly obtained bone marrow aspirates or peripheral blood draws. Clinical, prognostic, genetic, cytogenetic, and pathologic lab values as well as treatment and outcome data were manually curated from patient electronic medical records. Genetic characterization of the leukemia samples included results of a clinical deep-sequencing panel of genes commonly mutated in hematologic malignancies (Sequenome and GeneTrails (OHSU); Foundation Medicine (UTSW); Genoptix; and Illumina). Patient samples were cultured in RPMI with 10% FBS and 50% HS-5 conditioned media (ATCC) or SFEMII supplemented with 1x StemSpan CD34+ Expansion Media and 1 uM UM729 (StemCell Technologies).

Histology

Prior to staining, Kasumi-1 cells were treated with avapritinib (12 nM; Selleck) and/or ORY-1001 (12 nM; Selleck) for 72 h. Cells were prepared for CytoSpin 3 Shandon as described by manufacturer's protocol (ThermoShandon). Slides were fixed and stained using May-Grunwald Giemsa. Samples were imaged using Zeiss ApoTome housed in the Advanced Light Microscopy Core at OHSU.

Hematopoietic colony forming assay

Whole bone marrow was obtained (AllCells) and CD34+ cells were selected using CD34 MicroBead Kit (Miltenyi Biotec) according to manufacturer's instructions. For the colony assay, 2000 CD34+ cells were used per replicate and plated in MethoCult™ H4435 Enriched (StemCell Technologies). The four groups were treated with avapritinib (12 nM), ORY-1001 (12 nM), avapritinib and ORY-1001 (12 nM/drug), or DMSO. Plates were incubated for 14 days in 5% CO_2 and 37°C. Samples were imaged using STEMvision

(StemCell Technologies) and blinded prior to counting by another investigator by assigning letters randomly. ImageJ (NIH) was used to count colonies after blinding.

Drug Synergy

Drug synergy was assessed using an 8 x 8 matrix of drug concentrations. Cells were treated for 72 hours prior to MTS assay to evaluate viability. Cell viability was used to calculate drug synergy with SynergyFinder based on the ZIP reference model[20].

Flow Cytometry

To assess myeloid differentiation, Kasumi-1 cells were treated with 12 nM ORY-1001, 12 nM avapritinib, 12 nM ORY-1001/12 nM avapritinib or DMSO for 72 h. PerCP-e710 CD86 (Invitrogen) was used per the manufacture's protocol. To assess apoptosis, Kasumi-1 cells were treated with 12 nM ORY-1001, 36 nM avapritinib, 12 nM ORY-1001/36 nM avapritinib or DMSO for 48 h. APC Annexin V apoptosis detection kit (Invitrogen) was used according to the manufacture's protocol. For cell cycle analysis, Kasumi-1 cells were treated with 12 nM ORY-1001, 36 nM avapritinib, 12 nM ORY-1001/12 nM avapritinib or DMSO for 24, 48, and 72 h. Cells were fixed using ethyl alcohol and stained with propidium iodide (BioLegend). Strained cells were analyzed on a LSRFortessa flow cytometer (BD) housed in the OHSU Flow Cytometry Shared Resource.

RNA Interference

Two SMARTvector Inducible Human SPI1 hEF1a-TurboRFP shRNAs for SPI1/PU.1 were obtained from Horizon Discovery (230493625, 230705089). Lentivirus was produced by transfecting Lenti-X 293T cells (Clontech) with the SMARTvector transfer plasmid and packaging/pseudotyping plasmids. psPAX2 was a gift from Didier Trono (Addgene plasmid # 12260 ; http://n2t.net/addgene:12260 ; RRID:Addgene_12260) and pMD2.G was a gift from Didier Trono (Addgene plasmid # 12259 ; http://n2t.net/addgene:12259 ; RRID:Addgene_12259). The supernatants containing lentivirus was collected after 48 hours of culture and filtered with a 0.45 um filter. Kasumi-1 cells were transduced with virus via spinnoculation in the presence of polybrene. Transduced cells were selected with 1 ug/ml puromycin to produce a stable cell line.

Bulk RNA-sequencing

Kasumi-1 cells were treated with 12 nM GSK-LSD1, 12 nM avapritinib, 12 nM GSK-LSD1/12 nM avapritinib or DMSO for 12 h. Total RNA was isolated using a RNeasy Plus Mini Kit (Qiagen). BGI performed the library preparation and sequencing at 50 base pair (BP) paired end (PE). For the Kasumi-1 PU.1 KD experiment, cells were treated with 1 ug/ml doxycycline, 50 nM avapritinib, 1 ug/ml doxycycline/50 nM avapritinib, or DMSO for 24 hours. Total RNA was isolated with RNeasy Plus Mini Kit (Qiagen) and libraries were prepared with Zymo-Seq RiboFree Total RNA Library Kit (Zymo). The OHSU Massively Parallel Sequencing Shared Resource (MPSSR) performed the sequencing at 100 BP single end.

CUT&Tag

Kasumi-1 cells were treated with 12 nM GSK-LSD1, 12 nM avapritinib, 12 nM GSK-LSD1/12 nM avapritinib or DMSO for 24 hr. Benchtop CUT&Tag was performed as

previously described[21]. In brief, cells were counted, harvested, and centrifuged for 5 min at 300xg at room temperature. Cells were washed 2X in 1.5 mL wash buffer (20 mM HEPES pH 7.5, 150 mM NaCl, 0.5 mM Spermidine, 1× Protease inhibitor cocktail). Concanavlin A magnetic coated beads (Bangs Laboratories) were activated in binding buffer by washing 2X (20 mM HEPES pH 7.5, 10 mM KCl, 1 mM $CaCl_2$, 1 mM $MnCl_2$). Washed cells were separated into 100,000 cell aliquots and 10 ul of activated beads were added to each sample. Samples rotated end over end for 7 minutes at room temperature. A magnetic stand was used to separate beads, supernatant was removed. Primary antibody was diluted 1:50 in antibody buffer (20 mM HEPES pH 7.5, 150mM NaCl, 0.5 mM Spermidine, 1× Protease inhibitor cocktail, 0.05% digitonin, 2 mM EDTA, 0.1% BSA). The primary antibodies used were: H3K27Ac (ab4729, Abcam), H3K4me1 (#5326, Cell Signaling Technologies), H3K4me3 (#9751, Cell Signaling Technologies), and Normal Rabbit IgG (#2729, CST). Cells were incubated overnight at 4°C on a nutator. Primary antibody was replaced with a guinea-pig anti rabbit secondary antibody diluted to 1:100 in wash buffer (Antibodies Online). Samples were incubated for 45 minutes at room temperature on nutator. Secondary antibody was removed and samples were washed 2X in dig-wash buffer (20 mM HEPES pH 7.5, 150 mM NaCl, 0.5 mM Spermidine, 1× Protease inhibitor cocktail, 0.05% Digitonin). pA-Tn5 transposase, prepared and loaded with adaptors as previously described[21], was diluted 1:100 in dig-300 buffer (20 mM HEPES pH 7.5, 300 mM NaCl, 0.5 mM Spermidine, 1× Protease inhibitor cocktail, 0.01% digitonin) and added to samples. Samples were incubated for 1 hour at room temperature on nutator. Samples were washed 2X with dig-300 buffer then resuspended in tagmentation buffer (dig-300 buffer with 1 mM $MgCl_2$). Samples were incubated at 37°C for 1 hour. DNA was extracted with phenol:chloroform extraction. Samples were amplified by PCR using custom nextera primers at 400 nM and NEBNext HiFi 2x PCR Master Mix (New England Biolabs)[22]. PCR conditions were set to: 72°C for 5 minutes, 98°C for 30 seconds, 14 cycles of 98°C for 10 sec, 63°C for 10 sec, and 72°C for 1 minute. Libraries were purified with AMPure Beads (Beckman) and sequenced on a NextSeq 500 sequencer (Illumina) using 37 BP PE sequencing by MPSSR.

Kasumi-1 PU.1 sh401 cells were treated with 1 ug/ml doxycycline, 50 nM avapritinib, 1 ug/ml doxycycline/50 nM avapritinib, or DMSO for 24 hours. CUT&Tag was adapted from the benchtop version and was preformed similarly to the updated protocol[23]. Nuclei were prepared by incubating cell on ice for 10 minutes with NE1 buffer (20 mM HEPES-KOH pH 7.9, 10 mM KCl, 0.5 mM spermidine, 0.1% Triton X-100, 10% glycerol, 1x Protease inhibitor cocktail). Cells were centrifuged at 1300xg for 4 minutes at 4°C and supernatant was removed. Nuclei extract was resuspended in wash buffer (20 mM HEPES pH 7.5, 150 mM NaCl, 0.5 mM Spermidine, 1× Protease inhibitor cocktail) and 10% DMSO and frozen at -80°C. Briefly, 100,000 nuclei were thawed and incubated with 5 ul activated Concanavalin A beads (Bangs Laboratory) for 10 minutes at room temperature. Supernatant was removed and beads were resuspended in wash buffer. Samples were incubated with primary antibody diluted 1:100 in antibody buffer (wash buffer with 2 mM EDTA, 0.1% BSA) overnight at 4°C on the nutator. Primary antibody was removed, and beads incubated with guinea-pig anti rabbit secondary antibody diluted to 1:100 in wash buffer (Antibodies Online) for 30 minutes on nutator at room temperature. Beads were washed 2x with wash buffer. Beads incubated with pA-Tn5 (EpiCypher) diluted 1:20 in

300-wash buffer (20 mM HEPES pH 7.5, 300 mM NaCl, 0.5 mM Spermidine, 1× Protease inhibitor cocktail) for 1 h at room temperature on the nutator. Beads were washed 2x in 300-wash buffer and resuspended in tagmentation solution (300-wash buffer with 10 mM $MgCl_2$). Samples incubated at 37°C for 1 hour in a PCR cycler with heated lid then were washed 1x in TAPS wash buffer (10 mM TAPS, 0.2 mM EDTA). Beads were resuspended in 0.1% SDS release solution (0.1% SDS, 10 mM TAPS) and incubated for 1 hour at 58°C in a PCR cycler with heated lid. Triton neutralization solution (0.67% triton-X100) was added to bead slurry. Samples were amplified by PCR using custom nextera primers at 400 nM and NEBNext HiFi 2x PCR Master Mix (New England Biolabs)[22]. PCR conditions were set to: 58°C for 5 minutes, 72°C for 5 minutes, 98°C for 30 seconds, 12 cycles of 98°C for 10 sec, 60°C for 10 sec, and 72°C for 1 minute. Libraries were purified with HighPrep PCR Clean-up System (MagBio) and sequenced on a NextSeq 500 sequencer (Illumina) using 37 BP PE sequencing by MPSSR.

CUT&RUN

Kasumi-1 cells were treated with 12 nM GSK-LSD1, 12 nM avapritinib, 12 nM GSK-LSD1/12 nM avapritinib or DMSO for 12h or 24 h. CUT&RUN was performed as previously described[24]. Briefly, concanavlin A magnetic coated beads (Bangs Laboratories) were washed 2x in binding buffer (20 mM HEPES pH 7.5, 10 mM KCl, 1 mM $CaCl_2$, 1 mM $MnCl_2$) to activate. 500,000 cells per replicate were washed 2x with wash buffer (20 mM HEPES pH 7.5, 150 mM NaCl, 0.5 mM Spermidine, 1× Protease inhibitor cocktail). Cells were bound to beads by nutating for 10 minutes at room temperature. Cells were permeabilized and incubated over night at 4°C on nutator with primary antibody in antibody buffer (wash buffer, 0.001% digitonin, 3 mM EDTA). The following antibodies were used at 1:50: MYC (#13987, CST), PU.1 (MA5-15064, Invitrogen), LSD1 (ab17721, Abcam), GFI1 (ab21061, Abcam) and Normal Rabbit IgG (#2729, CST). Bead slurry was washed 2x with dig wash buffer (wash buffer, 0.001% dig) and resuspended with dig wash buffer and 1x pAG-MNase (Epicypher). Cell were incubated for 10 minutes on nutator at room temperature then washed 2x with dig wash buffer followed by resuspension in pAG-MNase reaction mix (dig wash buffer, 2 mM $CaCl_2$). Bead slurry was incubated for 2 hours at 4°C on nutator. STOP buffer (340 mM NaCl, 20 mM EDTA, 4 mM EGTA, 50 ug/mL RNase A, 50 ug/mL glycogen, 0.02% dig) was then added, then tubes were incubated at 37°C for 10 minutes. DNA was extracted using phenol:cholorform extraction. Libraries were prepared using NEBNext Ultra II DNA Library Prep Kit (NEB), modified for CUT&RUN as previously described[25]. After adapter ligation fragments were cleaned up with 1.75x AMPure beads (Beckman). Following PCR amplification, libraries were purified 2x with 1.2x AMPure beads to rid of adaptor fragments. Libraries were quantified on the 2100 Bioanalyzer instrument (Agilent) with the High Sensitivity DNA Analysis Kit (Agilent). Libraries were pooled and sequenced by MPSSR on a NextSeq 500 sequencer (Illumina) using 37 BP PE sequencing.

Western Blots

Kasumi-1 cells were treated with 12 nM ORY-1001, 12 nM avapritinib, 12 nM ORY-1001/12 nM avapritinib or DMSO for 24 h. Cells were lysed in 1x SDS sample buffer (25 mmol/L Tris (pH 6.8), 1% SDS, 5% glycerol, 3% β-mercaptoethanol, and 0.03% bromophenol blue) with sonication (50% amplitude, 2 – 15 second pulses). Samples were

spun at 14,000 x g for 10 minutes at 4°C then incubated for 5 minutes at 95°C. Samples were run on Criterion 4–15% Tris-HCl gradient gels (Bio-Rad). Gels were transferred to PVDF membranes, then blocked in Tris-buffered saline with 0.05% Tween (TBST) and 5% milk. Blots were probed with MYC (#13987, CST), PU.1 (MA5-15064, Invitrogen), or β-actin (#8457, CST) antibodies at 1:1000 in TBST overnight at 4°C. Membranes were incubated for 1 hour at room temperature with HRP-conjugated secondary antibody (CST, 7074S) at 1:5000. SuperSignal™ West Pico PLUS Chemiluminescent Substrate (ThermoFisher) was used to develop blots. Imaging was done on BioRad ChemiDoc Imaging System and analyzed using Image Lab (BioRad).

Reverse Phase Protein Array

Kasumi-1 cells were treated for 1 h and 24 h with avapritinib (100 nM) and ORY-1001 (12 nM). Cells were washed 2x in PBS then flash frozen. Cell pellets were lysed and processed by the University of Texas MD Anderson Cancer Center Functional Proteomics RPPA Core Facility.

ATAC sequencing

Patient sample 15-00807 was treated with 50 nM avapritinib, 50 nM ORY-1001, 50 nM avapritinib/50 nM ORY-1001, or DMSO for 24 hours. 50,000 cells per replicate were harvested for Fast-ATAC sequencing performed as previously described[26]. In brief, cells were resuspended in cold PBS and tagmentation master mix (25 ul of 2× tagmentation buffer, 2.5 ul of TDE1 [Illumina], 0.5 ul of 1% digitonin; 2x tagementation buffer: 66 mM Tris-Acetate, pH 7.8, 132 mM potassium acetate, 20 mM magnesium acetate, 32% v/v N,N-Dimethylformamide) was added. Samples were incubated at 37°C for 30 minutes. DNA was purified using Zymo Clean and Concentrator 5 Kit (Zymo). Transposed DNA was amplified and purified as described previously with adapted primers[27,28]. Samples were quantified using Qubit dsDNA HS Assay Kit (Invitrogen), pooled, and sequenced by Genewiz with a HiSeq-X (Illumina) using 75 BP PE sequencing.

Single Cell RNA Sequencing

Patient sample 14-00613 was treated with 12 nM ORY-1001, 12 nM avapritinib, 12 nM ORY-1001/12 nM avapritinib or DMSO for 24 hours then harvested. Cells were loaded onto the Chromium Controller (10X Genomics) according to the manufacturer's instructions. RNA libraries were prepared per the manufacturer's protocol, Chromium Next GEM Single Cell 3' Reagent v3.0 Kit (Biolegend, 10X Genomics). Libraries were sequenced on a HiSeq2500 (Illumina) using 100 BP PE sequencing.

Data Analysis

CUT&Tag and CUT&RUN Analysis

CUT&Tag and CUT&RUN libraries were aligned to the human genome (hg38) using Bowtie2[29] and the following options --local --very-sensitive-local --no-unal --no-mixed --no-discordant --phred33 -I 10 -X 700. Peaks were called using a custom script available upon request. High confidence peaks were defined by presence in 2/2 or 2/3 replicates. Consensus bed files were formed by merging the high confidence peaks from DMSO, avapritinib, ORY-1001, and combination using BEDTools[30]. Differential peaks were

identified using DESeq2[31] with default parameters. Heatmaps were produced using the ComplexHeatmap package from Bioconductor[32]. Peaks were annotated to the nearest feature using ChIPseeker[33]. GO analysis was performed using Genomic Regions Enrichment of Annotations Tool (GREAT)[34]. Counts tables for differential peaks were produced using multicov from BEDTools[30]. Counts per million (CPM) normalized tracks, global signal heatmaps, and plot profiles at specified regions were generated using DeepTools[35]. The DeepTools matrix was extracted and used to assess differences in H3K27Ac signal. Active promoters were defined by the presence of H3K4me3 and H3K27Ac within 1000 bp of a TSS. Active enhancers were defined by the presence of H3K4me1 and H3K27Ac beyond 1000 bp of a TSS. CPM normalized tracks were merged with bigWigMerge[36] and visualized using Integrative Genomics Viewer[37].

ATAC Analysis

ATAC libraries were aligned to the human genome (hg38) using BWA-MEM[38] and sorted using SAMtools[39]. Duplicates were marked with Sambamba[40], duplicates and mitochondrial reads were removed. CPM normalized tracks were generated with DeepTools[35]. Differential accessibility was assessed with DESeq2[31]. GO analysis was performed using GREAT[34]. CPM normalized tracks were merged with bigWigMerge[36] and visualized using Integrative Genomics Viewer[37].

Bulk RNA Sequencing Analysis

Raw reads were trimmed with Trimmomatic[41] and aligned with STAR[42]. Differential expression analysis was performed using DESeq2[31]. Raw p values were adjusted for multiple comparisons using the Benjamini-Hochberg method. GO analysis was performed using Enrichr[43] and Gene Set Enrichment Analysis (GSEA)[44].

Single Cell RNA Sequencing Analysis

Sequencing output from 10X mRNA sequencing libraries were aligned to human genome (hg38) using CellRanger. Filtered feature matrices were analyzed using Seurat[45]. Cells expressing greater than 20% mitochondrial RNA were excluded as non-viable. Data integration revealed seven transcriptional clusters. Cluster identity was established via expression of early (CD34, SOX4, ERG, MYB, and GATA2), mid (CEBPD), and late (LYZ, ITGAX, CD14) features of hematopoiesis.

Quantification and Statistical Analysis

Data are shown as mean ± SEM. Prism software (version 9.1; Prism Software Corp.) or RStudio was used to perform statistical analysis, which are described in the figure legends. All data were analyzed with Kolmogorov-Smirnov (KS) test or ANOVA followed by Holm-Sidak correction. For differential analysis of RNA-seq, CUT&Tag, CUT&RUN, and ATAC-seq P values were adjusted for repeated testing with a false discovery rate using the Benjamini-Hochberg method[46].

Data Availability

The Gene Expression Omnibus (GEO) accession number for all RNA-seq, CUT&Tag, CUT&RUN, ATAC-seq, and scRNA-seq reported in this paper is GSE182150.

Results

Characterization of synergistic cytotoxicity following KIT and LSD1 inhibition

Combined kinase and LSD1 inhibition shows promise as a therapeutic strategy in certain molecularly defined subsets of AML[13]. To investigate the applicability of this combined therapy strategy to KIT-mutant AML, we performed a drug synergy analysis on KIT mutant AML cell lines with KIT and LSD1 inhibitors. This revealed LSD1 inhibition, with GSK-LSD1 and ORY-1001, had minimal effect on cell viability as a single agent, but markedly potentiated the efficacy of avapritinib (Figure 1 A-D, Supplementary Figure 1 A). We confirmed these results in EOL-1 cells which are also sensitive to avapritinib due to having a PDGFRA translocation[47] (Supplementary Figure 1 B). A major concern of combination therapy is toxicity to normal tissues including the hematopoietic system. To evaluate the toxicity of this combination, we performed a hematopoietic colony forming assay using normal CD34+ cells in the presence of the single agents or the combination. LSD1 inhibition reduced colony formation by 33%, consistent with the know role of LSD1 in supporting multi-lineage hematopoiesis[48] (Figure 1 E). However, avapritinib did not depress colony formation alone and did not cause a further decrease in colony formation when combined with LSD1 inhibition. Furthermore, the drug combination failed to substantially alter the growth of leukemia cell lines without KIT mutations, arguing that the drug combination is specific to KIT mutant cells (Figure 1 F). To further characterize the response to combined inhibition of KIT and LSD1, we performed a flow cytometry-based apoptosis assay. After 48 hours of treatment, the combination group contained more PI+ (dead) and Annexin V+/PI- (early apoptosis) cells versus DMSO (Supplementary Figure 1 C-D). These results confirm that the drug combination produces greater cytotoxicity than either drug alone. In other molecular subtypes of AML, LSD1 inhibition promotes cell death through differentiation of immature AML blasts[13,49–53]. Surface expression of the maturation associated marker, CD86, was increased by LSD1 inhibitor alone and to a similar degree when combined with avapritinib (Supplementary Figure 1 E-F). However, this effect was modest and was not accompanied by significant morphologic differentiation after 72 hours of treatment (Supplementary Figure 1 G), in contrast to the effects seen in MLL-rearranged AML[52]. Overall, LSD1 inhibition potentiates the cytotoxic effect of avapritinib in KIT mutant CBF AML cell lines. This effect is specific to KIT mutant cells as the drug combination has limited impact on healthy bone marrow or KIT wild type leukemia lines. Finally, although there is some immunophenotypic evidence of differentiation with LSD1 inhibition, this is not modified by co-treatment with avapritinib, and is relatively modest compared with results obtained in MLL-rearranged models.

Combined KIT and LSD1 inhibition leads to repression of MYC targets and activation of PU.1 targets

To investigate the mechanism of synergy between LSD1 inhibition and KIT inhibition, we performed RNA-sequencing (RNA-seq) on Kasumi-1 cells treated with avapritinib, GSK-LSD1, or the combination. Unsupervised clustering was performed on all differentially expressed genes to assess patterns of expression (Figure 2 A; Supplementary Table 1). Clusters 2 and 3 showed increased expression with the combination compared to either single agent, whereas clusters 5 and 6 showed decreased expression with the combination (Figure 2 B-C; Supplementary Table 1). We leveraged pathway analysis to identify

biological programs that could drive the different expression patterns. Clusters 1 and 2 revealed enrichment for *SPI1* (PU.1) target genes, a transcription factor (TF) involved in hematopoietic differentiation (Figure 2 B)[54]. Conversely, analysis of clusters 5 and 6 was highly enriched for MYC (a key regulator of proliferation and cell survival) target genes (Figure 2 C)[55]. Taken together, increased expression of PU.1 target genes and downregulation of MYC target genes are features of the synergistic effect of avapritinib and LSD1 inhibition.

Decreased activation of MYC bound promoters involved in cellular proliferation

Given the transcriptional impact of combined LSD1 and KIT inhibition on MYC target genes, we hypothesized MYC binding may be altered by the drug combination. To that end, we performed Cleavage Under Targets and Release Using Nuclease (CUT&RUN) to evaluate changes in MYC binding with drug treatment. While LSD1 inhibition alone modestly decreased global MYC binding, a greater decrease was observed with the drug combination (Figure 3 A). Consistent with this finding, MYC protein level also decreased with the drug combination (Supplementary Figure 2 A). The majority of high confidence MYC peaks localized to promoter regions, suggesting MYC-dependent transcriptional regulation commonly occurs at promoters (Figure 3 B). Given the decreased transcript abundance of MYC target genes (Figure 2 A), we hypothesized that MYC would predominantly localize to the transcription start sites (TSS) of down regulated genes. Indeed, MYC is enriched at the TSSs of genes with decreased expression in response to the drug combination (Figure 3 C). With LSD1 inhibition alone and combined KIT/LSD1 inhibition, MYC binding decreases at the TSSs of down regulated genes. To assess whether this loss of MYC binding was associated with decreased promoter activity, we assessed H3K27Ac read pileup at MYC bound promoters using cleavage under targets and tagmentation (CUT&Tag). Using H3K4me3 and H3K27Ac, we identified 9,369 active promoters (Supplementary Figure 3 B; Supplementary Table 2). With dual LSD1 and KIT inhibition there is a significant decrease in acetylation at MYC bound promoters (adj p-value < 2.2e-16) (Figure 3 D, Supplementary Figure 3 C; Supplementary Table 3). GO analysis of MYC bound promoters revealed an enrichment for proliferation related genes such as CDK13 and several ribosomal components (Figure 3 D, Supplementary Figure 2 D). Altogether, combined inhibition of LSD1 and KIT results in decreased total MYC protein, a loss of MYC binding, and decreased activation of genes involved in cell growth. To test if this altered gene expression program changes cell growth and division, we used a flow cytometry-based assay to evaluate changes in cell cycle. After 24, 48, and 72 hours of treatment, the drug combination significantly decreased the percentage of cycling cells and increased the percentage of cells in G1 phase (Supplementary Figure 3 A-B). In sum, LSD1 and KIT inhibition results in loss of MYC binding and decreased acetylation of proliferation associate promoters ultimately leading to cell cycle arrest.

Combined KIT and LSD1 inhibition cause activation of GFI1 and LSD1 bound enhancers

The transcriptional response to combined KIT and LSD1 inhibition involves both repression of MYC target genes as well as activation of differentiation-associated genes. In other subtypes of AML, differentiation of AML blasts is a major driver of drug responses. A key driver of this differentiation response is displacement of the repressive transcription factor GFI1 from chromatin. GFI1 and LSD1 co-bind and pharmacologic inhibition of

LSD1 results in a loss of GFI1 binding and activation of repressed enhancers of differentiation associated genes[50]. To evaluate the role of GFI1 in the response to combined KIT and LSD1 inhibition in KIT mutant AML, we assessed genome-wide binding of GFI1 and LSD1 by CUT&RUN. LSD1 binding did not change after treatment in any treatment condition (Supplementary Figure 4 A). GFI1 binding decreased with LSD1 inhibition (Supplementary Figure 3 A), but was lost to a greater degree with the drug combination. To assess whether this loss of GFI1 binding was associated with activation of the underlying enhancers, we used CUT&Tag to identify enhancers, marked by the presence of H3K4me1. Using this approach, we identified 4,199 active enhancers (Supplementary Figure 2 B; Supplementary Table 2). The enhancers bound by GFI1 and LSD1 showed subtle changes in the underlying H3K27Ac, however these changes were modest compared with the results seen in MLL rearranged AML treated with LSD1 inhibitors, arguing that other factors are the major drivers of the response to combined KIT and LSD1 (Supplementary Figure 4 B; Supplementary Table 4)[50]. Indeed, this is consistent with the relatively modest immunophenotypic differentiation and absence of morphologic differentiation driven by drug treatment (Supplementary Figure 1I).

LSD1 inhibition leads to loss of PU.1 at MYC +26 kb *enhancer*

PU.1 has also been implicated as a regulator of LSD1 inhibitor responses and PU.1 target genes are featured prominently in our RNA-seq analysis[52] (Figure 2 A). We therefore performed CUT&RUN to profile the genome wide binding of PU.1 (Figure 4 A). PU.1 binding is completely lost after treatment with LSD1 inhibition without changes in total PU.1 protein (Figure 4 A, Supplemental Figure 5 A). Annotation of PU.1 binding sites revealed localization outside of promoter regions (Figure 4 B). To assess whether loss of PU.1 activity was sufficient to augment the cytotoxicity of KIT inhibition, we used both a pharmacologic inhibitor of PU.1 activity (DB2313) and a doxycycline-inducible short hairpin RNA (shRNA) targeting PU.1. In both instances, we found a dose-dependent increase in KIT inhibitor potency with increasing PU.1 inhibition or knockdown (KD) (Figure 4 D, Supplementary Figure 5 B-C). Next, we tested whether PU.1 KD and KIT inhibition recapitulates the transcriptional consequences of LSD1 and KIT inhibition. Bulk RNA-seq of Kasumi-1 cells treated with avapritinib and PU.1 shRNA showed a depletion of MYC target genes by gene set enrichment analysis (Figure 4 E; Supplementary Table 5). The genes from this MYC target geneset showed more repression with the combination than with either drug alone (Figure 4 F). These data demonstrate that a loss of PU.1 activity contributes to the repression of MYC target genes. To understand how PU.1 KD regulates MYC expression, we performed CUT&Tag for H3K27Ac. Acetylation of the MYC promoter significantly decreased with PU.1 KD and KIT inhibition (adj p-value = 0.03) (Figure 4 G; Supplementary Table 6). Interestingly, no PU.1 peak was identified at the MYC promoter. However, a PU.1 peak was identified at the annotated +26 Kb enhancer downstream of the MYC gene[56], which was marked by both H3K27Ac and H3K4me1 (Figure 4 G). Consistent with the global changes in PU.1 binding, PU.1 signal was lost with LSD1 inhibition and PU.1 KD resulted in a significant loss of H3K27Ac which further decreased with KIT inhibition (adj p-value = 0.01). Interestingly, LSD1 and GFI1 are found at the MYC promoter, but they were not identified at the +26 Kb enhancer (Supplementary Figure 5 D). These data demonstrate that PU.1 activates MYC transcription through a downstream

enhancer. When PU.1 binding is lost with LSD1 inhibition, MYC gene activation is reduced resulting in decreased transcription of MYC target genes (Figure 4 H).

KIT and LSD1 inhibition destabilizes MYC and repress LSD1 target genes through PI3K/AKT pathway

MYC is a key regulator of cellular proliferation and survival, among other functions, thus its transcription, activation, and stability are carefully regulated[57]. KIT activates both MAPK/RAS/ERK and PI3K/AKT pathways each contributing to MYC stability[58]. We hypothesized KIT inhibition may alter MYC stability, leading to reduced MYC binding. To assess the changes in these signaling pathways, we performed reverse phase protein array (RPPA) on Kasumi-1 cells treated with the single drugs or the combination. CausalPath phosphoprotein activity network revealed decreased activation of AKT upstream of decreased total MYC protein (Supplementary Figure 6 A,B; Supplementary Table 7). To understand the dynamics of AKT signaling after combined KIT and LSD1 inhibition, we used a heatmap to visualize individual members of the PI3K/AKT pathway[59–61] (Figure 5 A,B; Supplementary Figure 6 C). After 1 h of treatment with KIT inhibition and the combination, total MYC protein and serine phosphorylated GSK3a/b (pS21) decreased markedly. Serine 21 of GSK3a/b is phosphorylated by AKT, resulting in inhibition of kinase activity (Figure 5 B). Active (dephosphorylated) GSK3a/b phosphorylates MYC to destabilize the protein[62]. Following KIT and LSD1 inhibition, PI3K/AKT is downregulated resulting in the reactivation of GSK3a/b, thus destabilizing MYC protein.

As LSD1 inhibition potentiates the cytotoxic effects of avapritinib, we hypothesized that LSD1 might also interact with the KIT/AKT/GSK3 axis. Indeed, in glioblastoma cells (GSC11), GSK3b phosphorylates LSD1 resulting in activation[63]. This finding suggests KIT inhibition could increase the activity of LSD1, potentially increasing the dependency on this pathway and rendering cells more sensitive to LSD1 inhibition. To test this, we identified two gene-sets of LSD1 responsive genes: genes that increase in expression with LSD1 inhibition (LSD1-repressed) and genes that decrease in expression with LSD1 inhibition (LSD1-activated). We then assessed gene set enrichment of these LSD1 responsive genes in cells responding to KIT inhibition. Consistent with the hypothesis that KIT and LSD1 inhibition exert opposing effects on LSD1 target genes, we observed that avapritinib resulted in activation of LSD1-activated genes and repression of LSD1-repressed genes (Figure 5 C; Supplementary Table 8). We next compared the effect of LSD1 inhibition alone to combined KIT and LSD1 inhibition. With or without KIT inhibition, LSD1 inhibition resulted in activation of LSD1-repressed genes. However, LSD1-activated genes were only repressed by LSD1-inhibitor monotherapy but not when combined with KIT inhibition. These data support a model in which KIT inhibition suppresses MYC activity but activates LSD1 as a drug escape mechanism. This adaptive response to KIT inhibition can be targeted with the addition of LSD1 inhibitor, potentiating cell death (Figure 5 D).

We also investigated signaling responses to KIT and LSD1 inhibition at a later timepoint. At 24h, we observed that avapritinib-treated cells demonstrated increased levels of phospho-AKT (both pS473 and pT308) (Supplementary Figure 6 C). Kit protein

abundance was also upregulated at this time-point suggesting that upregulation of KIT may drive this later adaptive response. The addition of LSD1 inhibitor resulted in marked suppression of KIT protein abundance as well as phospho-AKT. Collectively, these results demonstrate a coordinated interplay between signaling pathways downstream of KIT (namely PI3K/AKT) and LSD1. Our data demonstrate that LSD1 inhibition targets many of the adaptive responses to KIT inhibition, potentially decreasing the propensity for cancer cell persistence.

LSD1 and KIT inhibition is synergistically cytotoxic in KIT mutant patient samples through MYC network repression

To verify our findings in cell lines in primary AML samples, we identified thirteen samples from the Beat AML cohort with KIT mutations.[64] Ten of the thirteen patient samples had mutations at D816, leading to ligand independent activation that is amenable to inhibition by avapritinib. Six of those patient samples had frozen viable cells available, four of which thawed with sufficient viability for further assays (Supplementary Table 9). We elected to evaluate transcriptional and epigenetic changes at 24 hours and drug synergy after 72 hours (Figure 6 A). Of the four patient samples, three responded with synergistic cytotoxicity to the LSD1 and KIT inhibitor (Figure 6 B, Supplementary Figure 7 A-C). Sample 17-00007 was from a relapsed patient and still showed synergistic response to LSD1 and KIT inhibition (Supplementary Figure 7 B). Sample 17-01023 did not respond, but only had a KIT mutant VAF of 6% arguing that this mutation only exists in a small subclone (Supplementary Figure 7 C). In sample 14-00613, bulk RNA-seq revealed a depletion of MYC target genes and cell cycle related genes (Figure 6 C-D; Supplementary Table 10). These transcriptional changes after dual drug treatment provide supporting evidence for suppression of MYC activity playing a key role in the response to LSD1 and KIT inhibition. Due to the epigenetic modifying role of LSD1, we were interested to know if dual inhibition of LSD1 and KIT altered the epigenetic landscape in patient samples. We used Transposase Accessible Chromatin using sequencing (ATAC-seq) to look at changes in chromatin accessibility in sample 15-00807[27]. Differential accessibility analysis revealed 1457 regions with significantly decreased accessibility after dual LSD1 and KIT inhibition. Gene Ontology analysis of these regions revealed enrichment for genes controlling cell cycle, including EEF2K, a kinase involved in cell cycle[65] (adj p-value = 0.0004) (Figure 6 E, Supplementary Figure 7 D; Supplementary Table 11). In sum, LSD1 and KIT inhibition is synergistically cytotoxic to patient samples with KIT mutations. With these samples, we confirm MYC target and cell cycle repression through transcriptomics and epigenetic changes.

LSD1 and KIT inhibition results in decreased MYC expression along single cell differentiation trajectory

Recent work using single cell RNA sequencing (scRNA-seq) has revealed that AML cells show substantial heterogeneity in differentiation status, existing along a differentiation continuum[66]. Cells at different relative positions on this trajectory may respond differently to treatment; however, these differences cannot be appreciated through bulk analysis. Therefore, we performed scRNA-seq to understand the transcriptional response of different cell populations within patient sample 14-00613. This analysis revealed six transcriptionally-defined clusters (Figure 7 A; Supplementary Table 12). These clusters were

classified using features of early (CD34, SOX4, ERG, MYB, and GATA2), mid (CEBPD), and late (LYZ, ITGAX, CD14) maturation (Figure 7 B, Supplementary Figure 8 A). Given the evidence of MYC and MYC target repression as a key response to dual inhibition of LSD1 and KIT, we assessed MYC expression across the myeloid trajectory (Figure 7 C-D). With combined KIT and LSD1 inhibition relative to DMSO control treatment, average MYC expression was decreased in undifferentiated cells (cluster 0) and MYC was detected in fewer cells. A similar response occurs in mid-trajectory cells (cluster 2). Taken together, dual inhibition of LSD1 and KIT in a KIT-mutant patient sample results in decreased MYC expression in immature cells. This single cell RNA-seq analysis further supports MYC regulation as a key driver of the response to dual LSD1 and KIT inhibition.

Discussion

The present work offers mechanistic insight into the synergistic dual inhibition of LSD1 and KIT, providing rational for evaluating the combination in patient with KIT mutant AML. The standard of care treatment for patients with KIT mutant AML involves induction and consolidation with cytarabine-based chemotherapy[67]. Following treatment, patients with CBF AML harboring mutant KIT have higher risk of relapse compared to CBF AML alone, thus the need for improved therapeutic options[68]. In this study, we evaluated dual inhibition of LSD1 and KIT as a novel combination therapy for KIT mutant AML. We show that combined inhibition of LSD1 and KIT is synergistically cytotoxic to AML cell lines harboring KIT mutations. Bulk RNA-seq revealed dysregulation of MYC and PU.1 (SPI1) transcriptional networks following combination treatment. Dual inhibition of LSD1 and KIT resulted in a loss of MYC binding and a loss of activating H3K27Ac at cell cycle genes, driving cell cycle exit. Furthermore, we identified a previously unappreciated role for PU.1 in driving MYC expression. Inhibition of LSD1 results in a global loss of PU.1 binding, including loss at the +26 kb MYC enhancer. This loss of PU.1 binding results in decreased enhancer acetylation and a corresponding decrease in MYC gene expression driving cell cycle exit. Dual LSD1 and KIT inhibition is also cytotoxic in AML patient samples with KIT mutations, with transcriptional and epigenetic profiling confirming the findings from cell lines. Our studies reveal that modulation of MYC and PU.1 transcriptional networks is a key feature of dual LSD1 and KIT inhibition, providing pre-clinical rational for early phase clinical trials investigating this combination in KIT mutant AML.

Our data identified a prominent role for MYC as a principal driver of the response to combined KIT and LSD1 inhibition. Prior work has established that KIT signaling regulates MYC protein stability through both the MAPK/RAS/ERK and PI3K/AKT pathways[69]. ERK phosphorylates and stabilizes MYC protein whereas PI3K/AKT restrains GSK-3b from phosphorylating and destabilizing MYC[58]. Our data shows that KIT inhibition results in decreased MYC protein, DNA binding and target gene expression. Additionally, we observed this effect is potentiated by LSD1 inhibition. LSD1 is bound to the MYC promoter and may play a direct role in the activation of MYC gene expression. Alternatively, LSD1 may repress negative regulators of MAPK/ERK or PI3K/AKT pathway with LSD1 inhibition resulting in decreased pathway activation and a resultant loss of MYC activity. Indeed, inhibition of LSD1 leads to upregulation of PIK3IP1, a negative regulator of AKT signaling that may potentiate the effects of KIT inhibition[70]. Finally, we

provide evidence that LSD1 inhibition alters PU.1 dependent activation of the +26kb MYC enhancer, leading to a loss of MYC gene expression. Further elucidating which of these mechanisms are most critical for LSD1-dependent regulation of MYC will be an important avenue for future investigation.

PU.1 has previously been implicated as a key determinant of LSD1 inhibitor responses in MLL-rearranged AML, with LSD1 inhibition leading to activation of PU.1 bound enhancers[50,52]. Consistent with this, our RNA-seq shows that PU.1 targets are activated with combined KIT and LSD1 inhibition. Interestingly, genome wide profiling of PU.1 binding revealed loss of PU.1 binding with LSD1 inhibition. Together these data suggest that PU.1 serves as a transcriptional repressor at a large number of genes. In contrast, at the +26 kB MYC enhancer, PU.1 loss is accompanied by a loss of H3K27Ac and corresponding decrease in MYC expression suggesting transactivation activity. Depending on the context, PU.1 can act as a repressor or activator[71,72]. In normal hematopoiesis RUNX1 and PU.1 bind together to activate transcription; however, RUNX1-ETO acts as a corepressor to PU.1[73]. When PU.1 binding is lost due to LSD1 inhibition, it is likely reactivating genes that were repressed by PU.1/RUNX1-ETO. At other loci, our data suggest PU.1 serves as a transcriptional activator, likely through interactions with coactivators, such as histone acetyl transferases[74]. We identified an enhancer downstream of MYC that is bound by PU.1. When PU.1 is knocked-down, as a model for PU.1 binding loss, we observed a decrease in acetylation at the enhancer and promoter of MYC. We hypothesize that loss of activating PU.1 complexes at this MYC enhancer leads to a loss of MYC expression and cell cycle exit. The underlying mechanism of PU.1 suppression by LSD1 inhibition is not evident in our study as LSD1 and PU.1 are not co-bound, suggesting an intermediate step contributing to transcriptional regulation, such as post-translational modifications. PU.1 is phosphorylated at Ser148[75,76] leading to increased activity and DNA binding. Additionally, LSD1 is known to demethylate non-histone protein substrates and potentially could also regulate transcription factors such as PU.1 in this manner. The precise mechanism of LSD1-dependent suppression of PU.1 activity in KIT-mutant AML remains an important area for future investigation.

GFI1 has been identified as a repressive transcription factor that co-binds with LSD1[50]. Disruption of the LSD1-GFI1 complex has been implicated as a key mechanism of LSD1 inhibitor response in MLL-rearranged AML resulting in enhancer activation and subsequent differentiation[50]. We confirmed that LSD1 inhibition also evicts GFI1 from chromatin in KIT mutant AML, but found that this loss of GFI1 binding did not substantially alter the activity of underlying enhancers. We did identify numerous regions of differential chromatin remodeling and gene activation in response to LSD1 inhibition, arguing that additional factors are also crucial for driving drug responses. Indeed, prior studies have nominated numerous other transcription factors as key regulators of the effect of LSD1 inhibitor including CEBPA, PU.1 and MYB[50]. Our results suggest that GFI1 dependent gene regulation may play a more prominent role in MLL-rearranged AML than KIT mutant AML. It is unknown if GFI1 contributes to changes in MYC and PU.1 transcriptional networks in KIT mutant AML, and remains a key area for future study.

Collectively, our results demonstrate dual inhibition of KIT and LSD1 is synergistically cytotoxic in KIT mutant AML cell lines and in primary patient samples. Given the propensity for KIT-mutant AML to relapse after standard of care treatment, many experts support bone marrow transplantation for such patients in first remissions, although this has not yet become the standard of care. A less toxic treatment approach would be of high clinical value for patients of advanced age or significant co-morbidities. We show here that combined KIT and LSD1 inhibition is highly effective against KIT mutant AML, suggesting this approach could be added to standard of care treatment to decrease relapse rates or could be used in the salvage setting for individuals with relapsed disease not eligible for intensive chemotherapy. Furthermore, we identify changes in the PU.1 and MYC transcriptional networks as key biomarkers of drug efficacy. Assessment of the activity of these key transcriptional nodes could be a valuable correlate for on-target drug activity during clinical investigation. In total, our results support the investigation of combined KIT and LSD1 inhibition in early phase clinical trials for patients with KIT-mutant AML.

Acknowledgements

We thank the following OHSU core facilities for their assistance: Advanced Light Microscopy, Flow Cytometry Shared Resource, ExaCloud Cluster Computational Resource, and the Advanced Computing Center. Funding was provided by an American Society of Hematology Research Restart Award, an American Society of Hematology Scholar Award and 1 K08 CA245224 from NCI awarded to T.P.B. The Functional Proteomics RPPA Core is supported by MD Anderson Cancer Center Support Grant # 5 P30 CA016672-40.

Author contributions

B.M.S., T.P.B., D.J.C., B.J.D., and J.E.M. designed research; B.M.S. and T.P.B. performed research; B.M.S., T.P.B., J.V., G.L.K., W.Y., W.H., D.J.C., J.E., and T.A.L. contributed new reagents/analytic tools; B.M.S., T.P.B., B.J.D., and J.E.M. analyzed data; B.M.S and T.P.B. wrote the manuscript; B.M.S, T.P.B., and J.E.M. reviewed and revised the manuscript.

Conflict of interest

B.J.D. -- SAB: Aileron Therapeutics, Therapy Architects (ALLCRON), Cepheid, Vivid Biosciences, Celgene, RUNX1 Research Program, EnLiven Therapeutics, Gilead Sciences (inactive), Monojul (inactive); SAB & Stock: Aptose Biosciences, Blueprint Medicines, Iterion Therapeutics, Third Coast Therapeutics, GRAIL (SAB inactive); Scientific Founder: MolecularMD (inactive, acquired by ICON); Board of Directors & Stock: Amgen; Board of Directors: Burroughs Wellcome Fund, CureOne; Joint Steering Committee: Beat AML LLS; Founder: VB Therapeutics; Clinical Trial Funding: Novartis, Bristol-Myers Squibb, Pfizer; Royalties from Patent 6958335 (Novartis exclusive license) and OHSU and Dana-Farber Cancer Institute (one Merck exclusive license). J.E.M. -- SAB: Ionis pharmaceuticals. The other authors do not have conflicts of interest, financial or otherwise.

References

1. Kelly, L. M. & Gilliland, D. G. Genetics of myeloid leukemias. *Annu. Rev. Genomics Hum. Genet.* **3**, 179–198 (2002).

2. Scheijen, B. & Griffin, J. D. Tyrosine kinase oncogenes in normal hematopoiesis and hematological disease. *Oncogene* **21**, 3314–3333 (2002).

3. Gilliland, D. G. & Griffin, J. D. The roles of FLT3 in hematopoiesis and leukemia. *Blood* **100**, 1532–1542 (2002).

4. Bullinger, L., Döhner, K. & Döhner, H. Genomics of Acute Myeloid Leukemia Diagnosis and Pathways. *J. Clin. Oncol.* **35**, 934–946 (2017).

5. Corces-Zimmerman, M. R., Hong, W.-J., Weissman, I. L., Medeiros, B. C. & Majeti, R. Preleukemic mutations in human acute myeloid leukemia affect epigenetic regulators and persist in remission. *Proc. Natl. Acad. Sci.* **111**, 2548–2553 (2014).

6. Ueyama, J. *et al.* [Treatment with a tyrosine-kinase inhibitor of for c-KIT mutation and AML1-ETO double positive refractory acute myeloid leukemia]. *Rinshō Ketsueki Jpn. J. Clin. Hematol.* **53**, 460–464 (2012).

7. Cairoli, R. *et al.* Imatinib mesylate in the treatment of Core Binding Factor leukemias with KIT mutations: A report of three cases. *Leuk. Res.* **29**, 397–400 (2005).

8. Megías-Vericat, J. E., Ballesta-López, O., Barragán, E., Martínez-Cuadrón, D. & Montesinos, P. Tyrosine kinase inhibitors for acute myeloid leukemia: A step toward disease control? *Blood Rev.* **44**, 100675 (2020).

9. Bewersdorf, J. P., Shallis, R., Stahl, M. & Zeidan, A. M. Epigenetic therapy combinations in acute myeloid leukemia: what are the options? *Ther. Adv. Hematol.* **10**, 2040620718816698 (2019).

10. Salamero, O. *et al.* First-in-Human Phase I Study of Iadademstat (ORY-1001): A First-in-Class Lysine-Specific Histone Demethylase 1A Inhibitor, in Relapsed or Refractory Acute Myeloid Leukemia. *J. Clin. Oncol.* **38**, 4260–4273 (2020).

11. Odenike, O. *et al.* Results from the first-in-human study of mivebresib (ABBV-075), a pan-inhibitor of bromodomain and extra terminal proteins, in patients with relapsed/refractory acute myeloid leukemia. *J. Clin. Oncol.* **37**, 7030–7030 (2019).

12. Dombret, H. *et al.* A Phase 1 Study of the BET-Bromodomain Inhibitor OTX015 in Patients with Advanced Acute Leukemia. *Blood* **124**, 117–117 (2014).

13. Braun, T. P. *et al.* Combined inhibition of JAK/STAT pathway and lysine-specific demethylase 1 as a therapeutic strategy in CSF3R/CEBPA mutant acute myeloid leukemia. *Proc. Natl. Acad. Sci.* (2020) doi:10.1073/pnas.1918307117.

14. Avellino, R. & Delwel, R. Expression and regulation of C/EBPα in normal myelopoiesis and in malignant transformation. *Blood* **129**, 2083–2091 (2017).

15. Speck, N. A. & Gilliland, D. G. Core-binding factors in haematopoiesis and leukaemia. *Nat. Rev. Cancer* **2**, 502–513 (2002).

16. Paschka, P. *et al.* Adverse Prognostic Significance of KIT Mutations in Adult Acute Myeloid Leukemia With inv(16) and t(8;21): A Cancer and Leukemia Group B Study. *J. Clin. Oncol.* **24**, 3904–3911 (2006).

17. Brizzi, M. F., Dentelli, P., Rosso, A., Yarden, Y. & Pegoraro, L. STAT Protein Recruitment and Activation in c-Kit Deletion Mutants. *J. Biol. Chem.* **274**, 16965–16972 (1999).

18. Larizza, L., Magnani, I. & Beghini, A. The Kasumi-1 cell line: a t(8;21)-kit mutant model for acute myeloid leukemia. *Leuk. Lymphoma* **46**, 247–255 (2005).

19. Lück, S. C. *et al.* KIT mutations confer a distinct gene expression signature in core binding factor leukaemia. *Br. J. Haematol.* **148**, 925–937 (2010).

20. Ianevski, A., Giri, A. K. & Aittokallio, T. SynergyFinder 2.0: visual analytics of multi-drug combination synergies. *Nucleic Acids Res.* **48**, W488–W493 (2020).

21. Kaya-Okur, H. S. *et al.* CUT&Tag for efficient epigenomic profiling of small samples and single cells. *Nat. Commun.* **10**, 1–10 (2019).

22. Buenrostro, J. D. *et al.* Integrated Single-Cell Analysis Maps the Continuous Regulatory Landscape of Human Hematopoietic Differentiation. *Cell* **173**, 1535-1548.e16 (2018).

23. Henikoff, S., Henikoff, J. G., Kaya-Okur, H. S. & Ahmad, K. Efficient chromatin accessibility mapping in situ by nucleosome-tethered tagmentation. *eLife* **9**, e63274 (2020).

24. Skene, P. J. & Henikoff, S. An efficient targeted nuclease strategy for high-resolution mapping of DNA binding sites. *eLife* **6**, e21856 (2017).

25. Liu, N. *et al.* Direct Promoter Repression by BCL11A Controls the Fetal to Adult Hemoglobin Switch. *Cell* **173**, 430-442.e17 (2018).

26. Corces, M. R. *et al.* Lineage-specific and single-cell chromatin accessibility charts human hematopoiesis and leukemia evolution. *Nat. Genet.* **48**, 1193–1203 (2016).

27. Buenrostro, J. D., Wu, B., Chang, H. Y. & Greenleaf, W. J. ATAC-seq: A Method for Assaying Chromatin Accessibility Genome-Wide. *Curr. Protoc. Mol. Biol.* **109**, 21.29.1-21.29.9 (2015).

28. Buenrostro, J. D. *et al.* Single-cell chromatin accessibility reveals principles of regulatory variation. *Nature* **523**, 486–490 (2015).

29. Langmead, B. & Salzberg, S. L. Fast gapped-read alignment with Bowtie 2. *Nat. Methods* **9**, 357–359 (2012).

30. Quinlan, A. R. & Hall, I. M. BEDTools: a flexible suite of utilities for comparing genomic features. *Bioinformatics* **26**, 841–842 (2010).

31. Love, M. I., Huber, W. & Anders, S. Moderated estimation of fold change and dispersion for RNA-seq data with DESeq2. *Genome Biol.* **15**, 550 (2014).

32. Gu, Z., Eils, R. & Schlesner, M. Complex heatmaps reveal patterns and correlations in multidimensional genomic data. *Bioinformatics* **32**, 2847–2849 (2016).

33. Yu, G., Wang, L.-G. & He, Q.-Y. ChIPseeker: an R/Bioconductor package for ChIP peak annotation, comparison and visualization. *Bioinformatics* **31**, 2382–2383 (2015).

34. McLean, C. Y. *et al.* GREAT improves functional interpretation of cis-regulatory regions. *Nat. Biotechnol.* **28**, 495–501 (2010).

35. Ramírez, F. *et al.* deepTools2: a next generation web server for deep-sequencing data analysis. *Nucleic Acids Res.* **44**, W160–W165 (2016).

36. Kuhn, R. M., Haussler, D. & Kent, W. J. The UCSC genome browser and associated tools. *Brief. Bioinform.* **14**, 144–161 (2013).

37. Robinson, J. T. *et al.* Integrative Genomics Viewer. *Nat. Biotechnol.* **29**, 24–26 (2011).

38. Li, H. & Durbin, R. Fast and accurate short read alignment with Burrows–Wheeler transform. *Bioinformatics* **25**, 1754–1760 (2009).

39. Li, H. *et al.* The Sequence Alignment/Map format and SAMtools. *Bioinformatics* **25**, 2078–2079 (2009).

40. Tarasov, A., Vilella, A. J., Cuppen, E., Nijman, I. J. & Prins, P. Sambamba: fast processing of NGS alignment formats. *Bioinformatics* **31**, 2032–2034 (2015).

41. Bolger, A. M., Lohse, M. & Usadel, B. Trimmomatic: a flexible trimmer for Illumina sequence data. *Bioinformatics* **30**, 2114–2120 (2014).

42. Dobin, A. *et al.* STAR: ultrafast universal RNA-seq aligner. *Bioinformatics* **29**, 15–21 (2013).

43. Kuleshov, M. V. *et al.* Enrichr: a comprehensive gene set enrichment analysis web server 2016 update. *Nucleic Acids Res.* **44**, W90–W97 (2016).

44. Subramanian, A. *et al.* Gene set enrichment analysis: A knowledge-based approach for interpreting genome-wide expression profiles. *Proc. Natl. Acad. Sci.* **102**, 15545–15550 (2005).

45. Butler, A., Hoffman, P., Smibert, P., Papalexi, E. & Satija, R. Integrating single-cell transcriptomic data across different conditions, technologies, and species. *Nat. Biotechnol.* **36**, 411–420 (2018).

46. Johnson, W. E., Li, C. & Rabinovic, A. Adjusting batch effects in microarray expression data using empirical Bayes methods. *Biostatistics* **8**, 118–127 (2007).

47. Evans, E. K. *et al.* A precision therapy against cancers driven by KIT/PDGFRA mutations. *Sci. Transl. Med.* **9**, (2017).

48. Kerenyi, M. A. *et al.* Histone demethylase Lsd1 represses hematopoietic stem and progenitor cell signatures during blood cell maturation. *eLife* **2**, e00633 (2013).

49. Harris, W. J. *et al.* The histone demethylase KDM1A sustains the oncogenic potential of MLL-AF9 leukemia stem cells. *Cancer Cell* **21**, 473–487 (2012).

50. Maiques-Diaz, A. *et al.* Enhancer Activation by Pharmacologic Displacement of LSD1 from GFI1 Induces Differentiation in Acute Myeloid Leukemia. *Cell Rep.* **22**, 3641–3659 (2018).

51. McGrath, J. P. *et al.* Pharmacological Inhibition of the Histone Lysine Demethylase KDM1A Suppresses the Growth of Multiple Acute Myeloid Leukemia Subtypes. *Cancer Res.* **76**, 1975–1988 (2016).

52. Cusan, M. *et al.* LSD1 inhibition exerts its antileukemic effect by recommissioning PU.1- and C/EBPα-dependent enhancers in AML. *Blood* **131**, 1730–1742 (2018).

53. Barth, J. *et al.* LSD1 inhibition by tranylcypromine derivatives interferes with GFI1-mediated repression of PU.1 target genes and induces differentiation in AML. *Leukemia* **33**, 1411–1426 (2019).

54. Moreau-Gachelin, F. Spi-1/PU.1: an oncogene of the Ets family. *Biochim. Biophys. Acta BBA - Rev. Cancer* **1198**, 149–163 (1994).

55. Eilers, M. & Eisenman, R. N. Myc's broad reach. *Genes Dev.* **22**, 2755–2766 (2008).

56. Fishilevich, S. *et al.* GeneHancer: genome-wide integration of enhancers and target genes in GeneCards. *Database J. Biol. Databases Curation* **2017**, (2017).

57. Sears, R. The Life Cycle of C-Myc: From Synthesis to Degradation. *Cell Cycle Georget. Tex* **3**, 1133–7 (2004).

58. Gregory, M. A., Qi, Y. & Hann, S. R. Phosphorylation by Glycogen Synthase Kinase-3 Controls c-Myc Proteolysis and Subnuclear Localization*. *J. Biol. Chem.* **278**, 51606–51612 (2003).

59. Manning, B. D. & Toker, A. AKT/PKB Signaling: Navigating the Network. *Cell* **169**, 381–405 (2017).

60. Darici, S. *et al.* Targeting PI3K/Akt/mTOR in AML: Rationale and Clinical Evidence. *J. Clin. Med.* **9**, (2020).

61. Peck, B., Ferber, E. C. & Schulze, A. Antagonism between FOXO and MYC Regulates Cellular Powerhouse. *Front. Oncol.* **3**, 96 (2013).

62. Sears, R. *et al.* Multiple Ras-dependent phosphorylation pathways regulate Myc protein stability. *Genes Dev.* **14**, 2501–2514 (2000).

63. Zhou, A. *et al.* Nuclear GSK3β promotes tumorigenesis by phosphorylating KDM1A and inducing its deubiquitylation by USP22. *Nat. Cell Biol.* **18**, 954–966 (2016).

64. Tyner, J. W. *et al.* Functional genomic landscape of acute myeloid leukaemia. *Nature* **562**, 526–531 (2018).

65. cdc2–cyclin B regulates eEF2 kinase activity in a cell cycle- and amino acid-dependent manner. *EMBO J.* **27**, 1005–1016 (2008).

66. van Galen, P. *et al.* Single-Cell RNA-Seq Reveals AML Hierarchies Relevant to Disease Progression and Immunity. *Cell* **176**, 1265-1281.e24 (2019).

67. Zhu, H.-H. *et al.* MRD-directed risk stratification treatment may improve outcomes of t(8;21) AML in the first complete remission: results from the AML05 multicenter trial. *Blood* **121**, 4056–4062 (2013).

68. Tarlock, K. *et al.* Functional Properties of KIT Mutations Are Associated with Differential Clinical Outcomes and Response to Targeted Therapeutics in CBF Acute Myeloid Leukemia. *Clin. Cancer Res.* **25**, 5038–5048 (2019).

69. Abbaspour Babaei, M., Kamalidehghan, B., Saleem, M., Huri, H. Z. & Ahmadipour, F. Receptor tyrosine kinase (c-Kit) inhibitors: a potential therapeutic target in cancer cells. *Drug Des. Devel. Ther.* **10**, 2443–2459 (2016).

70. Lee, K., Kitagawa, M., Liao, P. J., Virshup, D. M. & Lee, S. H. A Ras-LSD1 axis activates PI3K signaling through PIK3IP1 suppression. *Oncogenesis* **9**, 1–10 (2020).

71. van Riel, B. & Rosenbauer, F. Epigenetic control of hematopoiesis: the PU.1 chromatin connection. *Biol. Chem.* **395**, 1265–1274 (2014).

72. Minderjahn, J. *et al.* Mechanisms governing the pioneering and redistribution capabilities of the non-classical pioneer PU.1. *Nat. Commun.* **11**, 402 (2020).

73. Hu, Z. *et al.* RUNX1 regulates corepressor interactions of PU.1. *Blood* **117**, 6498–6508 (2011).

74. Bai, Y., Srinivasan, L., Perkins, L. & Atchison, M. L. Protein Acetylation Regulates Both PU.1 Transactivation and Igκ 3' Enhancer Activity. *J. Immunol.* **175**, 5160–5169 (2005).

75. Pongubala, J. M. R. *et al.* Effect of PU.1 Phosphorylation on Interaction with NF-EM5 and Transcriptional Activation. *Science* **259**, 1622–1625 (1993).

76. Rieske, P. & Pongubala, J. R. AKT Induces Transcriptional Activity of PU.1 through Phosphorylation-mediated Modifications within Its Transactivation Domain *. *J. Biol. Chem.* **276**, 8460–8468 (2001).

Figure Legends

Figure 1. Synergistic cytotoxicity of dual KIT and LSD1 inhibition in a KIT mutant AML cell line

A. Drug matrix of Kasumi-1 cells treated for 72 h with avapritinib and GSK-LDS1 or **B** ORY-1001 with synergy assessed by zero interaction potency (ZIP) score. **C.** Drug matrix of SKNO-1 cells treated for 72 h with avapritinib and ORY-1001 with synergy assessed by ZIP score. **D.** Viability assessment of K562, MOLM13, and CMK cells treated for 72 h with avapritinib and ORY-1001. **E.** IC50 of avapritinib with different concentrations of ORY-1001 in Kasumi-1 cells treated for 72 h; one-way ANOVA with Holm-Sidak correction. **F.** Colony assay using healthy CD34+ cells in, treated for 14 days with avapritinib (12 nM) and/or ORY-1001 (12 nM); two-way ANOVA with Holm-Sidak correction. (*$p < 0.05$)

Figure 2. Activation of PU.1 and repression of MYC target genes following KIT and LSD1 inhibition

A. RNA-seq performed on Kasumi-1 cells treated with avapritinib (12 nM) and/or GSK-LSD1 (12 nM) for 12 h (n=3/group). Genes with significant differential expression are displayed by K-means clustering. **B, C** Gene ontology analysis of clusters 2/ 3 and 5/6 from A.

Figure 3. Repression of MYC bound promoters of cell cycle related programs

A. Kasumi cells were treated for 24 h with avapritinib (12 nM) and/or GSK-LSD1 (12 nM; LSD1i) then subject to CUT&RUN (n=2/group). Heatmaps of global signal for MYC at high confidence consensus peaks (peak apex $\pm$ 1 kb). **B.** Annotation of consensus MYC peaks. **C.** MYC signal at TSSs of down or up regulated genes defined by RNA-seq. **D.** H3K27Ac signal at all MYC bound promoters in Kasumi-1 cells after 24 hours of treatment with avapritinib (12 nM) and/or GSK-LSD1 (12 nM; LSD1i). **E**. Gene ontology term enrichment for MYC bound promoters.

Figure 4. Loss of PU.1 binding at MYC enhancer resulting in loss of MYC enhancer and promoter activation

A. Kasumi cells were treated for 24 h with avapritinib (12 nM) and/or GSK-LSD1 (12 nM; LSD1i) then subject to CUT&RUN (*n*=2/group). Heatmaps of global signal for PU.1 at high confidence consensus PU.1 peaks (peak apex ± 1 kb). **B.** Annotation of high confidence consensus PU.1 peaks. **C.** Western blot of PU.1 in Kasumi-1 shRNA knockdown cells treated with and without 1 ug/ml doxycycline for 48 h. **D**. Drug matrix of avapritinib and doxycycline on Kasumi-1 PU.1 sh401 cells treated for 72 h. Synergy assessed by ZIP scores. **E.** Select depleted gene sets from bulk RNA-seq on PU.1 sh401, induced with doxycycline (1 ug/ul) 48 h before treatment with avapritinib (50 nM) for 24 h. NES = normalized enrichment score ($q < 0.05$). GSEA *p* value calculated by empirical permutation test and FDR adjusted. **F**. Normalized expression of MYC targets up gene set for DMSO, avapritinib (12 nM), PU.1 sh401 (1 ug/ml doxycycline), or both (*n*=3/group). **G**. Kasumi-1 cells with 24 h treatment with avapritinib (50 nM) and/or doxycycline (1 ug/ml) to induce PU.1 knockdown were used to perform CUT&Tag for H3K27Ac (*n*=3/group). H3K4me1 and PU.1 signal from above datasets in Kasumi-1 cells. Visualization of +26 Kb MYC. Both enhancer and MYC promoter lose acetylation. **H**. Model describing effect of loss of PU.1 and MYC binding after dual LSD1 and KIT inhibition. PU.1 no longer activates MYC promoter resulting in decreased MYC protein, leading to decreased expression of MYC target genes including those involved with cell proliferation.

Figure 5. KIT and LSD1 inhibition led to repression of LSD1 target genes and reverses activation of LSD1 target genes through KIT inhibition alone

A. Depiction of PI3K/AKT signaling pathway[59–61]. **B.** RPPA of Kasumi-1 cells treated for 1 h with avapritinib (100 nM) and/or ORY-1001 (12 nM). Heatmap of the normalized signal from PI3K/AKT pathway members. **C.** GSEA using genesets curated by bulk RNA-seq of Kasumi-1 cells treated for 12 h with GSK-LSD1 (12 nM). Genes repressed by LSD1 have significantly increased expression after LSD1 inhibition. Genes activated by LSD1 have significantly decreased expression after LSD1 inhibition. NES = normalized enrichment score ($q < 0.05$). GSEA *p* value calculated by empirical permutation test and FDR adjusted. **D.** Inhibition of KIT or LSD1 lead to opposing effect on LSD1 activity via the PI3K/AKT pathway. Dual inhibition results in repression of Myc and activation of genes natively repressed by LSD1.

Figure 6. KIT and LSD1 inhibition synergistically target KIT mutant AML patient samples resulting in decreased MYC and cell cycle programs

A. Experimental strategy for KIT mutant patient samples. Frozen viable samples were cultured ex vivo and treated for 24 h before bulk RNA-seq and ATAC-seq. For synergy analysis, samples were drug treated for 72 hours before assessing drug synergy. **B.** Drug matrix of patient sample 14-00613 treated for 72 h with avapritinib and ORY-1001 with synergy assessed by ZIP score. **C, D.** Select depleted gene sets from bulk RNA-seq on 14-00613 treated with avapritinib (50 nM) and ORY-1001 (12 nM) or DMSO for 24 h. NES = normalized enrichment score ($q < 0.05$). GSEA *p* value calculated by empirical permutation test and FDR adjusted. **E.** Differential analysis of bulk ATAC-seq on

15-00807 treated with avapritinib (50 nM) and ORY-1001 (50 nM) compared to DMSO. Enrichment of GO terms for regions with significantly decreased accessibility.

Figure 7. Varied degrees of MYC loss along the differentiation trajectory post LSD1 and KIT inhibition

A. Single cell RNA-seq on patient sample 14-00613 treated with ORY-1001 (12 nM) and/or avapritinib (12 nM) for 24 h. UMAP clustering of single cell gene expression. Clustering was performed on an integrated object that included cells treated with DMSO, avapritinib, ORY-1001, or the combination. **B.** Detected levels of CD34 (early) and CD14 (late) in integrated object to show differentiation trajectory from single cell analysis in A. **C.** MYC single cell gene expression in DMSO, ORY-1001 (LSD1i), avapritinib, and the combination from single cell analysis in A. **D.** Dot plot portraying the average gene expression and percentage of cells with MYC detected per UMAP cluster in A.

Supplementary Figure 1. Characterization of specificity and response of KIT and LSD1 inhibition

A. Viability assessment for Kasumi-1 cells treated for 72 h with avapritinib and ORY-1001 at different concentrations. Values normalized to average of viability of cells with highest dose of both drugs. **B.** Drug matrix of EOL-1 cells treated for 72 h with avapritinib and ORY-1001 with synergy assessed by ZIP score. **C, D**. Apoptosis flow cytometry of Kasumi-1 cells treated for 48 h with avapritinib (36 nM) and/or ORY-1001 (12 nM) as a percent of the parent population and representative plots of PI and Annexin V for each condition; two-way ANOVA with Holm-Sidak correction. **E, F.** Flow cytometric assessment of CD86 of Kasumi-1 cells treated for 72 h with avapritinib (12 nM) and/or ORY-1001 (12 nM). Representative histogram of CD86 signal with gray line representing CD86 positive gate and bar graph of CD86 signal for all replicates; one-way ANOVA with Holm-Sidak correction. **G.** Cytospin of Kasumi-1 cells treated for 72 h with avapritinib (12 nM) and/or ORY-1001 (12 nM), stained with May Grunwald-Giemsa. Scale bar represents 10 um. (* $p < 0.05$, ** $p < 0.01$, *** $p < 0.001$, **** $p < 0.0001$)

Supplementary Figure 2. Loss of total MYC protein and acetylation at MYC bound promoters

A. Western blot of total MYC and loading control in Kasumi-1 cells 24 h after treatment with avapritinib (12 nM) and/or ORY-1001 (12 nM; LSD1i). **B.** Venn diagram of peaks from Kasumi-1 CUT&Tag used to define regulatory elements. Promoters defined as H3K4me3 peaks within 1 kb from a TSS; enhancers defined as H3K4me1 peaks beyond 1 kb of a TSS. Regulatory elements that overlap with H3K27Ac are defined as active (n=2/group). **C.** Box and whisker plot of H3K27Ac signal at MYC bound promoters. KS used to assess differences. **D.** Example of lost acetylation at MYC bound promoter of CDK13.

Supplementary Figure 3. Decreased cell cycle progression with combined LSD1 and KIT inhibition

A, B. Cell cycle flow cytometry assay with PI of Kasumi-1 cells treated for 24, 48, or 72 h with avapritinib (12 nM) and/or ORY-1001 (12 nM). Bar chart of percentage of cells

within G1, S, or G2 phase and pie chart of percent of cells within each phase of cell cycle (n=3/group). * $p < 0.05$, ** $p < 0.01$, **** $p < 0.0001$

Supplementary Figure 4. Activation of LSD1 and GFI1 bound enhancers with KIT and LSD1 inhibition
A. Kasumi-1 cells were treated for 12 h (LSD1) or 24 h (GFI1) with avapritinib (12 nM) and/or LSD1 inhibitor (12 nM; ORY-1001 and GSK-LSD1 respectively) then subject to CUT&RUN (n=2-3/group). Heatmaps of global signal for LSD1 and GFI1 at their respective high confidence consensus peak sets (peak apex $\pm$ 1 kb). **B.** Peak profile and plot of H3K27Ac signal at active enhancers bound by LSD1 and GFI1 in Kasumi-1 cells after 24 hours of treatment with avapritinib (12 nM) and/or GSK-LSD1 (12 nM; LSD1i).

Supplementary Figure 5. PU.1 inhibition and knock down synergize with KIT inhibition
A. Western blot of total PU.1 and loading control in Kasumi-1 cells following 24 hour of treatment with avapritinib (12 nM) and/or ORY-1001 (12 nM). **B, C.** Drug matrix of Kasumi-1 cells treated for 72 h with avapritinib and DB2313 or doxycycline with synergy assessed by ZIP. **D.** GFI1 and LSD1 CUT&RUN tracks at MYC promoter.

Supplementary Figure 6. Identify AKT as prominent pathway leading to MYC repression
A. CausalPath analysis of RPPA results of Kasumi-1 cells treated for 24 h with avapritinib (100 nM) and/or ORY-1001 (12 nM) or DMSO. **B.** CausalPath analysis of RPPA as in A after 1 h of drug exposure. **C**. Heatmap of the normalized signal for PI3K/AKT pathway members after 24 h of drug exposure.

Supplementary Figure 7. Additional KIT and LSD1 inhibitor synergy plots in KIT mutant AML patient samples
A-C. Drug matrices of patient samples 15-00807, 17-00007, and 17-0123 treated for 72 h with avapritinib and ORY-1001 with synergy assessed by ZIP score. **D.** Example of decreased accessibility at cell cycle associated locus, EEF2K, from bulk ATAC-seq in 15-00807.

Supplementary Figure 8. Single cell RNA-seq markers for differentiation
A. Integrated single cell RNA-seq object showing the expression of differentiation markers. Markers were used to identify early, mid, and late stages of hematopoiesis in patient sample 14-00613

Figure 1

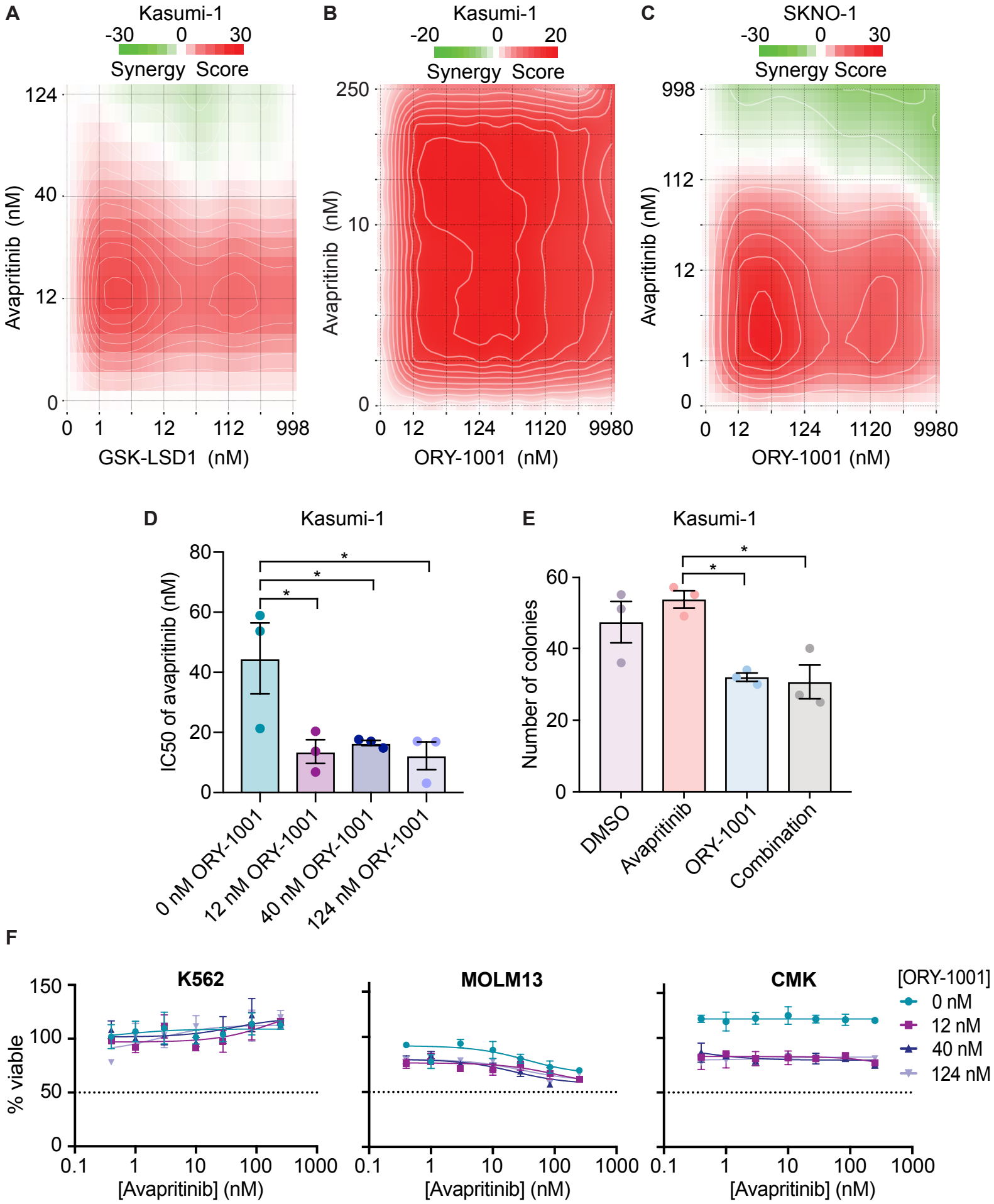
A
Kasumi-1
-30 0 30
Synergy Score
124
40
12
0
Avapritinib (nM)
0 1 12 112 998
GSK-LSD1 (nM)
B
Kasumi-1
-20 0 20
Synergy Score
250
10
0
Avapritinib (nM)
0 12 124 1120 9980
ORY-1001 (nM)
C
SKNO-1
-30 0 30
Synergy Score
998
112
12
1
0
Avapritinib (nM)
0 12 124 1120 9980
ORY-1001 (nM)
D
Kasumi-1
IC50 of avapritinib (nM)
80
60
40
20
0
*
*
*
0 nM ORY-1001
12 nM ORY-1001
40 nM ORY-1001
124 nM ORY-1001
E
Kasumi-1
Number of colonies
60
40
20
0
*
*
DMSO
Avapritinib
ORY-1001
Combination
F
K562
MOLM13
CMK
% viable
150
100
50
0
0.1 1 10 100 1000
[Avapritinib] (nM)
[ORY-1001]
0 nM
12 nM
40 nM
124 nM

Figure 2

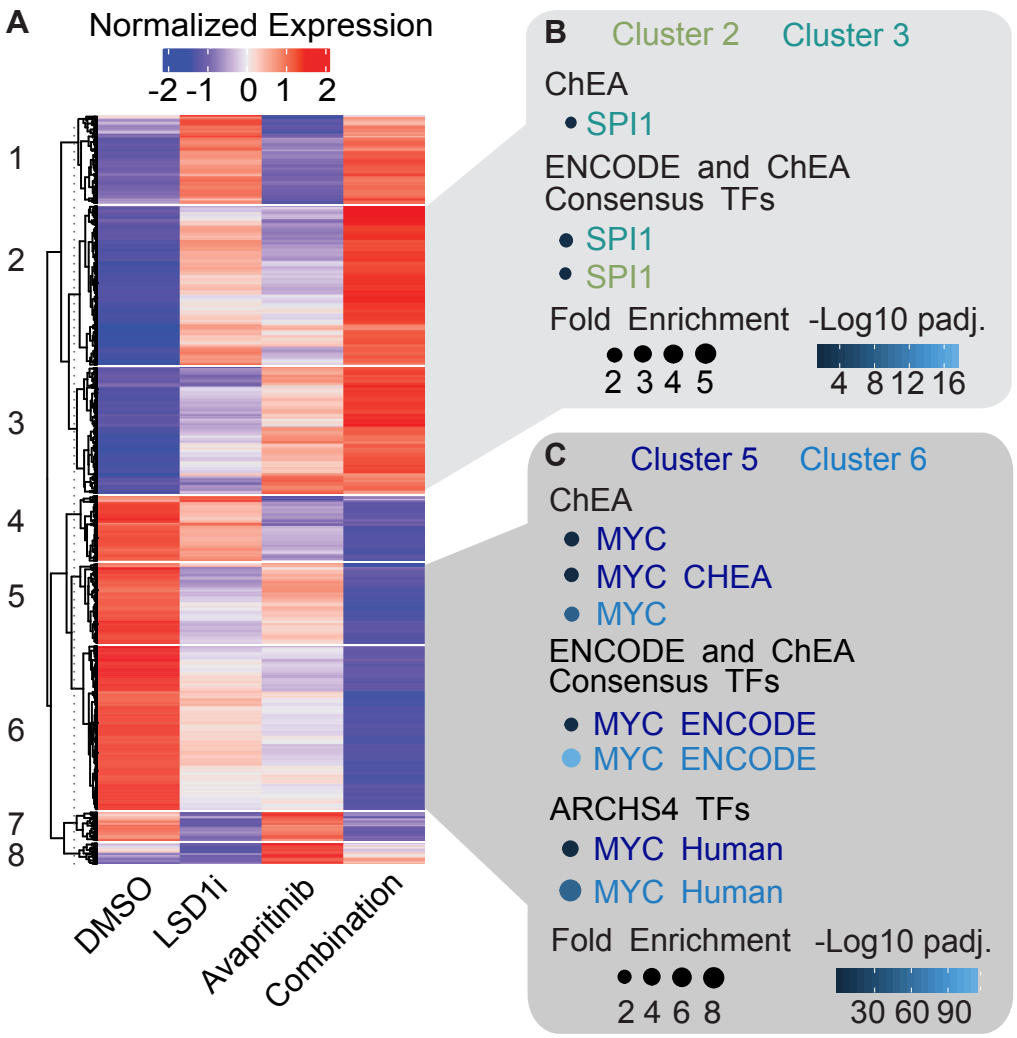
A
Normalized Expression
-2 -1 0 1 2
1
2
3
4
5
6
7
8
DMSO
LSD1i
Avapritinib
Combination
B
Cluster 2
Cluster 3
ChEA
SPI1
ENCODE and ChEA Consensus TFs
SPI1
SPI1
Fold Enrichment
2 3 4 5
-Log10 padj.
4 8 12 16
C
Cluster 5
Cluster 6
ChEA
MYC
MYC CHEA
MYC
ENCODE and ChEA Consensus TFs
MYC ENCODE
MYC ENCODE
ARCHS4 TFs
MYC Human
MYC Human
Fold Enrichment
2 4 6 8
-Log10 padj.
30 60 90

Figure 3

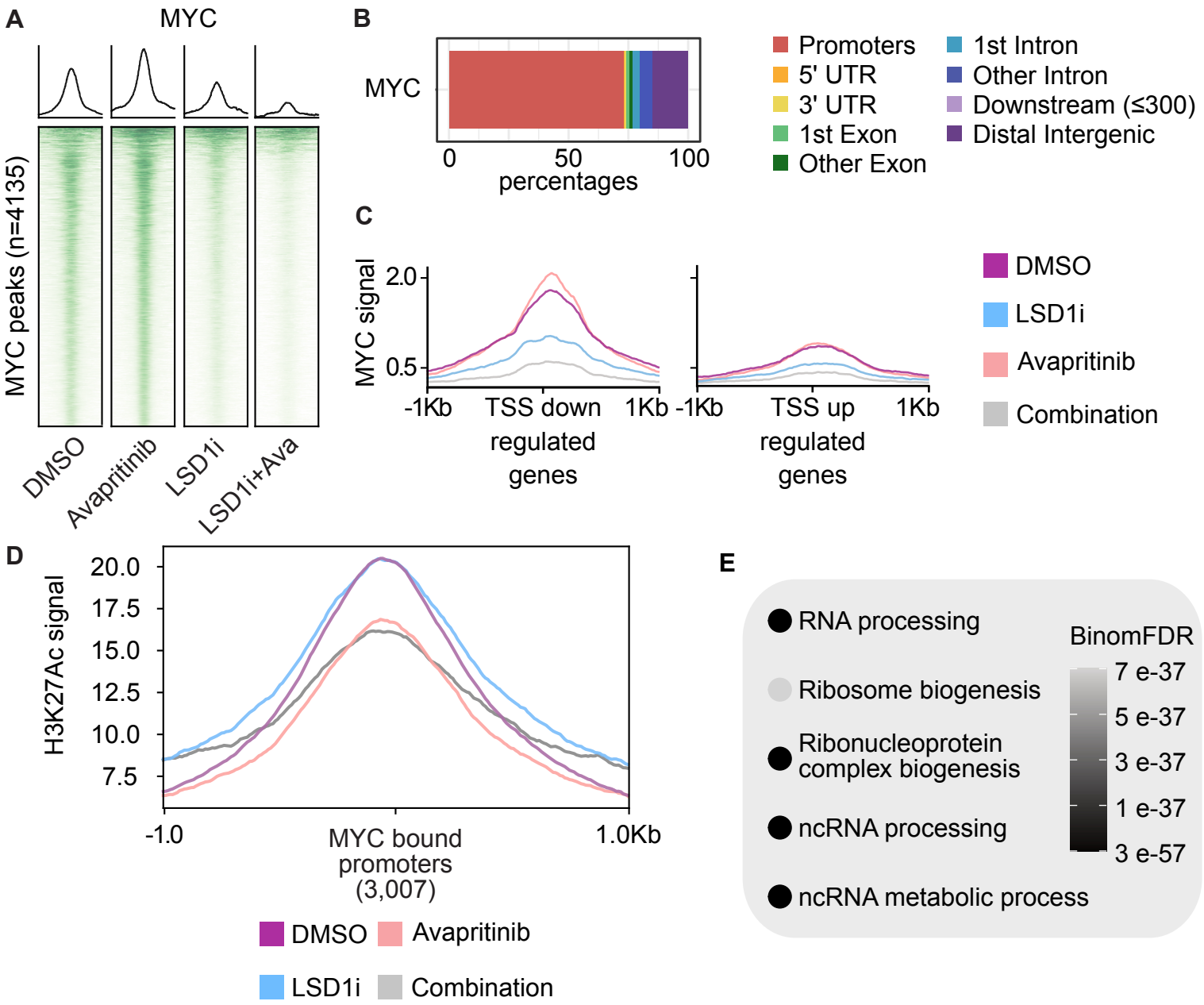
A
MYC
MYC peaks (n=4135)
DMSO
Avapritinib
LSD1i
LSD1i+Ava
B
MYC
0
50
100
percentages
Promoters
5' UTR
3' UTR
1st Exon
Other Exon
1st Intron
Other Intron
Downstream (≤300)
Distal Intergenic
C
MYC signal
2.0
0.5
-1Kb
TSS down regulated genes
1Kb
-1Kb
TSS up regulated genes
1Kb
DMSO
LSD1i
Avapritinib
Combination
D
H3K27Ac signal
20.0
17.5
15.0
12.5
10.0
7.5
-1.0
MYC bound promoters (3,007)
1.0Kb
DMSO
Avapritinib
LSD1i
Combination
E
RNA processing
Ribosome biogenesis
Ribonucleoprotein complex biogenesis
ncRNA processing
ncRNA metabolic process
BinomFDR
7 e-37
5 e-37
3 e-37
1 e-37
3 e-57

Figure 4

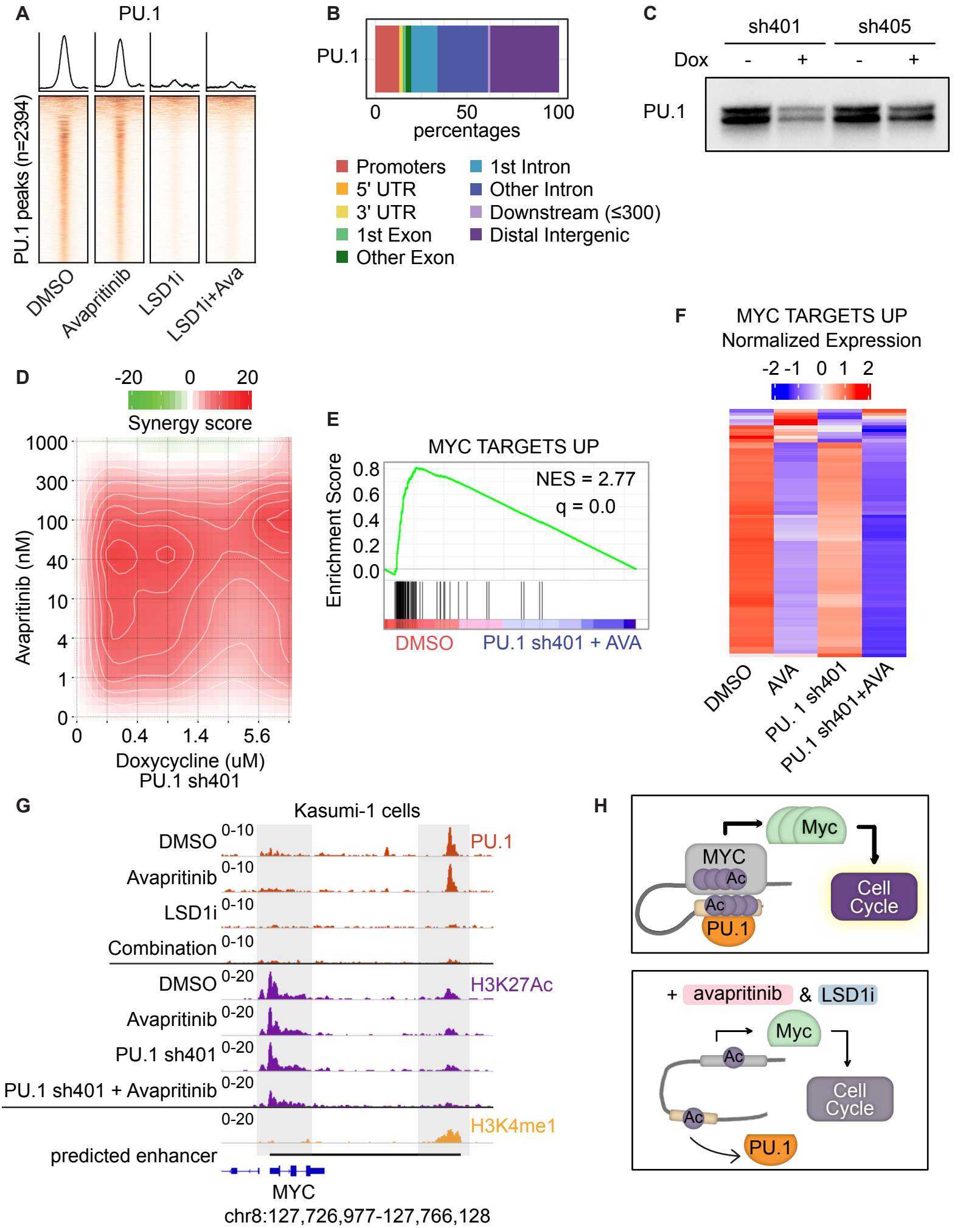
A
PU.1
PU.1 peaks (n=2394)
DMSO
Avapritinib
LSD1i
LSD1i+Ava
B
PU.1
0
50
100
percentages
Promoters
5' UTR
3' UTR
1st Exon
Other Exon
1st Intron
Other Intron
Downstream (≤300)
Distal Intergenic
C
sh401
sh405
Dox
-
+
-
+
PU.1
D
-20
0
20
Synergy score
1000
300
100
40
10
4
1
0
Avapritinib (nM)
0
0.4
1.4
5.6
Doxycycline (uM)
PU.1 sh401
E
MYC TARGETS UP
Enrichment Score
0.8
0.6
0.4
0.2
0.0
NES = 2.77
q = 0.0
DMSO
PU.1 sh401 + AVA
F
MYC TARGETS UP
Normalized Expression
-2 -1 0 1 2
DMSO
AVA
PU. 1 sh401
PU.1 sh401+AVA
G
Kasumi-1 cells
DMSO
Avapritinib
LSD1i
Combination
0-10
PU.1
DMSO
Avapritinib
PU.1 sh401
PU.1 sh401 + Avapritinib
0-20
H3K27Ac
0-20
H3K4me1
predicted enhancer
MYC
chr8:127,726,977-127,766,128
H
Myc
MYC
Ac
Ac
PU.1
Cell Cycle
+ avapritinib & LSD1i
Myc
Ac
Ac
Cell Cycle
PU.1

Figure 5

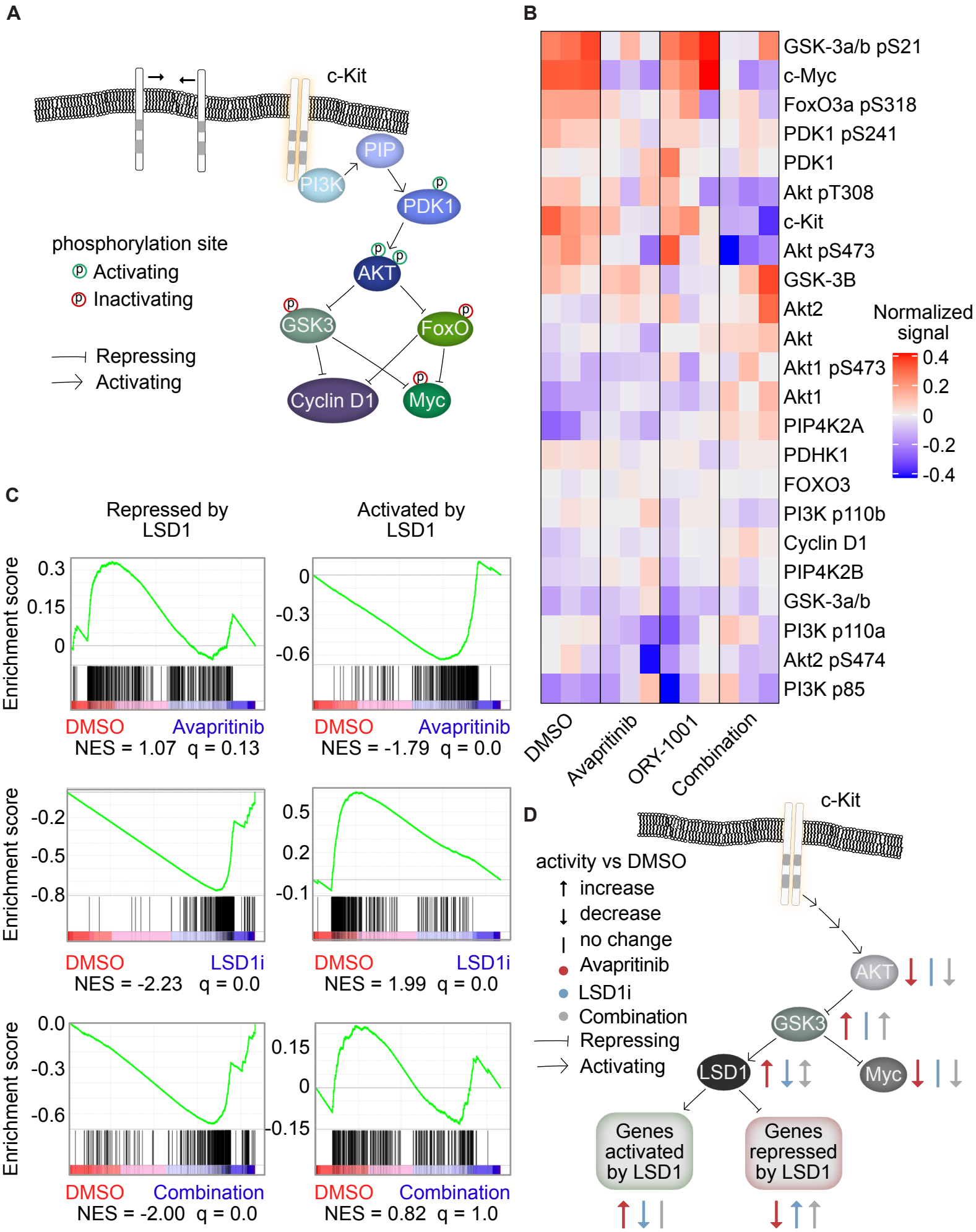
A
c-Kit
PIP
PI3K
PDK1
AKT
GSK3
FoxO
Cyclin D1
Myc
phosphorylation site
Activating
Inactivating
Repressing
Activating
B
GSK-3a/b pS21
c-Myc
FoxO3a pS318
PDK1 pS241
PDK1
Akt pT308
c-Kit
Akt pS473
GSK-3B
Akt2
Akt
Akt1 pS473
Akt1
PIP4K2A
PDHK1
FOXO3
PI3K p110b
Cyclin D1
PIP4K2B
GSK-3a/b
PI3K p110a
Akt2 pS474
PI3K p85
Normalized signal
0.4
0.2
0
-0.2
-0.4
DMSO
Avapritinib
ORY-1001
Combination
C
Repressed by LSD1
Activated by LSD1
Enrichment score
DMSO
Avapritinib
NES = 1.07 q = 0.13
NES = -1.79 q = 0.0
LSD1i
NES = -2.23 q = 0.0
NES = 1.99 q = 0.0
Combination
NES = -2.00 q = 0.0
NES = 0.82 q = 1.0
D
c-Kit
activity vs DMSO
increase
decrease
no change
Avapritinib
LSD1i
Combination
Repressing
Activating
AKT
GSK3
LSD1
Myc
Genes activated by LSD1
Genes repressed by LSD1

Figure 6

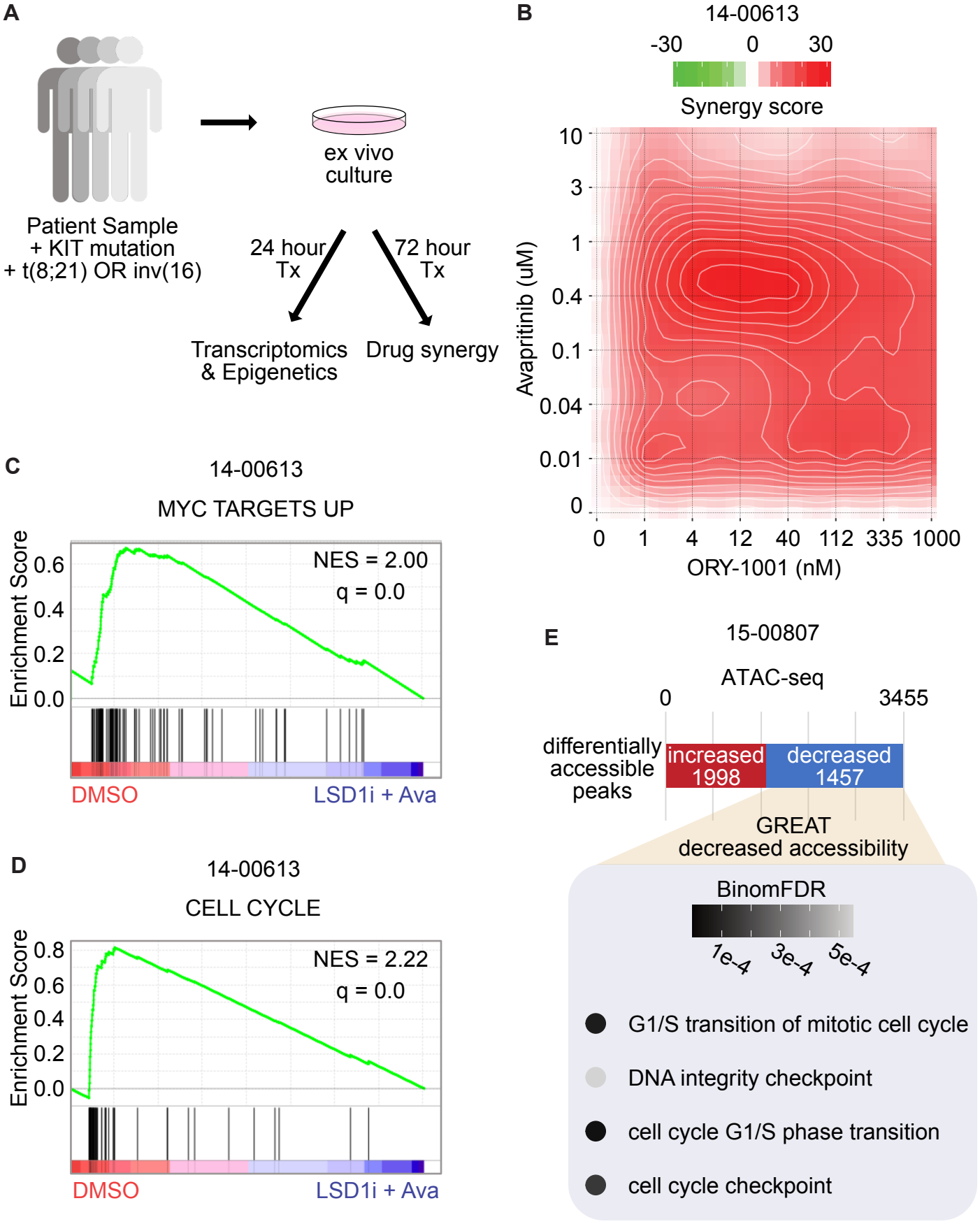
A
Patient Sample
+ KIT mutation
+ t(8;21) OR inv(16)
ex vivo
culture
24 hour
Tx
72 hour
Tx
Transcriptomics
& Epigenetics
Drug synergy
B
14-00613
-30
0
30
Synergy score
Avapritinib (uM)
10
3
1
0.4
0.1
0.04
0.01
0
0
1
4
12
40
112
335
1000
ORY-1001 (nM)
C
14-00613
MYC TARGETS UP
Enrichment Score
0.6
0.4
0.2
0.0
NES = 2.00
q = 0.0
DMSO
LSD1i + Ava
D
14-00613
CELL CYCLE
Enrichment Score
0.8
0.6
0.4
0.2
0.0
NES = 2.22
q = 0.0
DMSO
LSD1i + Ava
E
15-00807
ATAC-seq
0
3455
differentially
accessible
peaks
increased
1998
decreased
1457
GREAT
decreased accessibility
BinomFDR
1e-4
3e-4
5e-4
G1/S transition of mitotic cell cycle
DNA integrity checkpoint
cell cycle G1/S phase transition
cell cycle checkpoint

Figure 7

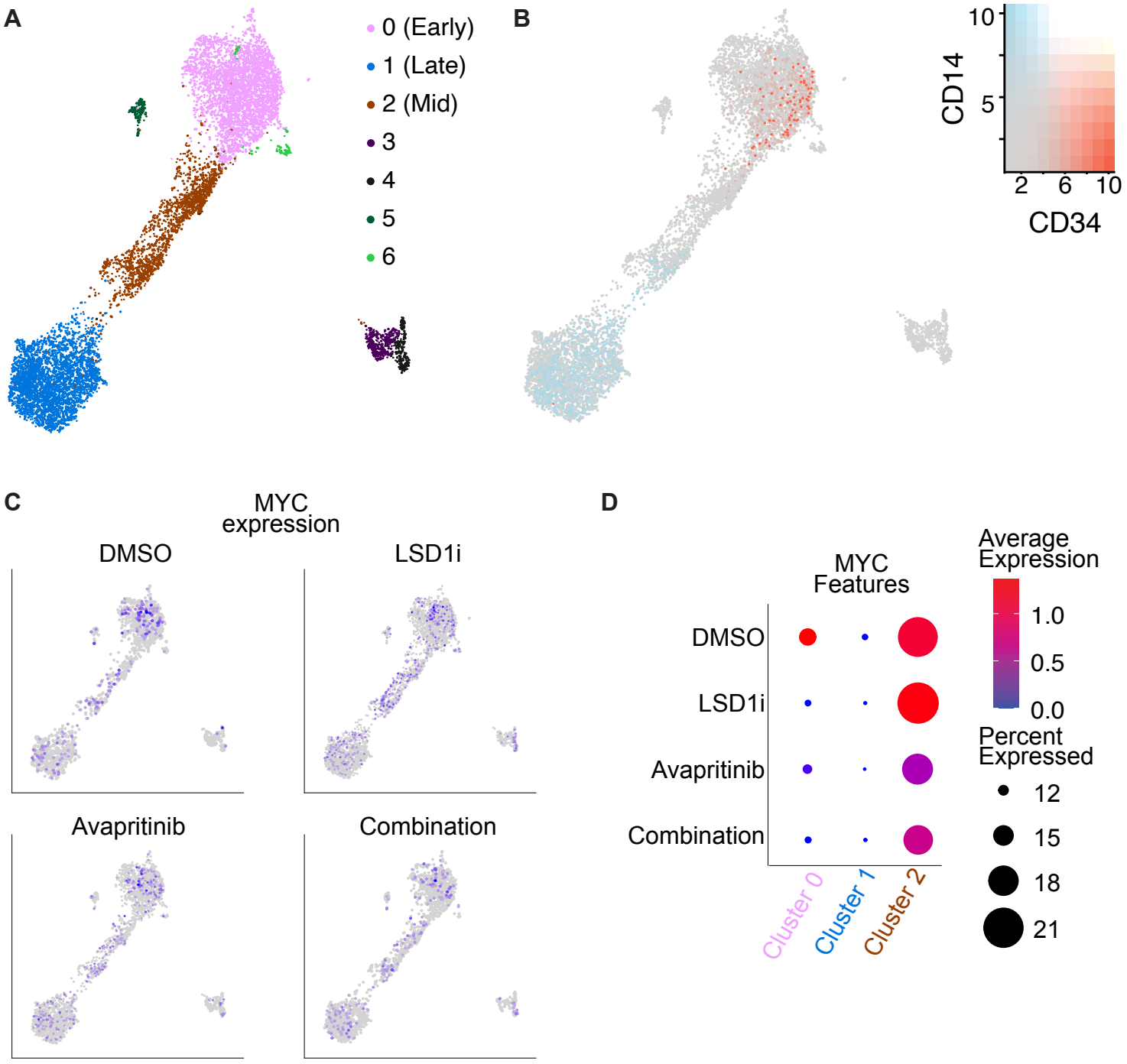
A
0 (Early)
1 (Late)
2 (Mid)
3
4
5
6
B
CD14
10
5
2
6
10
CD34
C
MYC
expression
DMSO
LSD1i
Avapritinib
Combination
D
MYC
Features
DMSO
LSD1i
Avapritinib
Combination
Cluster 0
Cluster 1
Cluster 2
Average
Expression
1.0
0.5
0.0
Percent
Expressed
12
15
18
21

Supplementary Figure 1

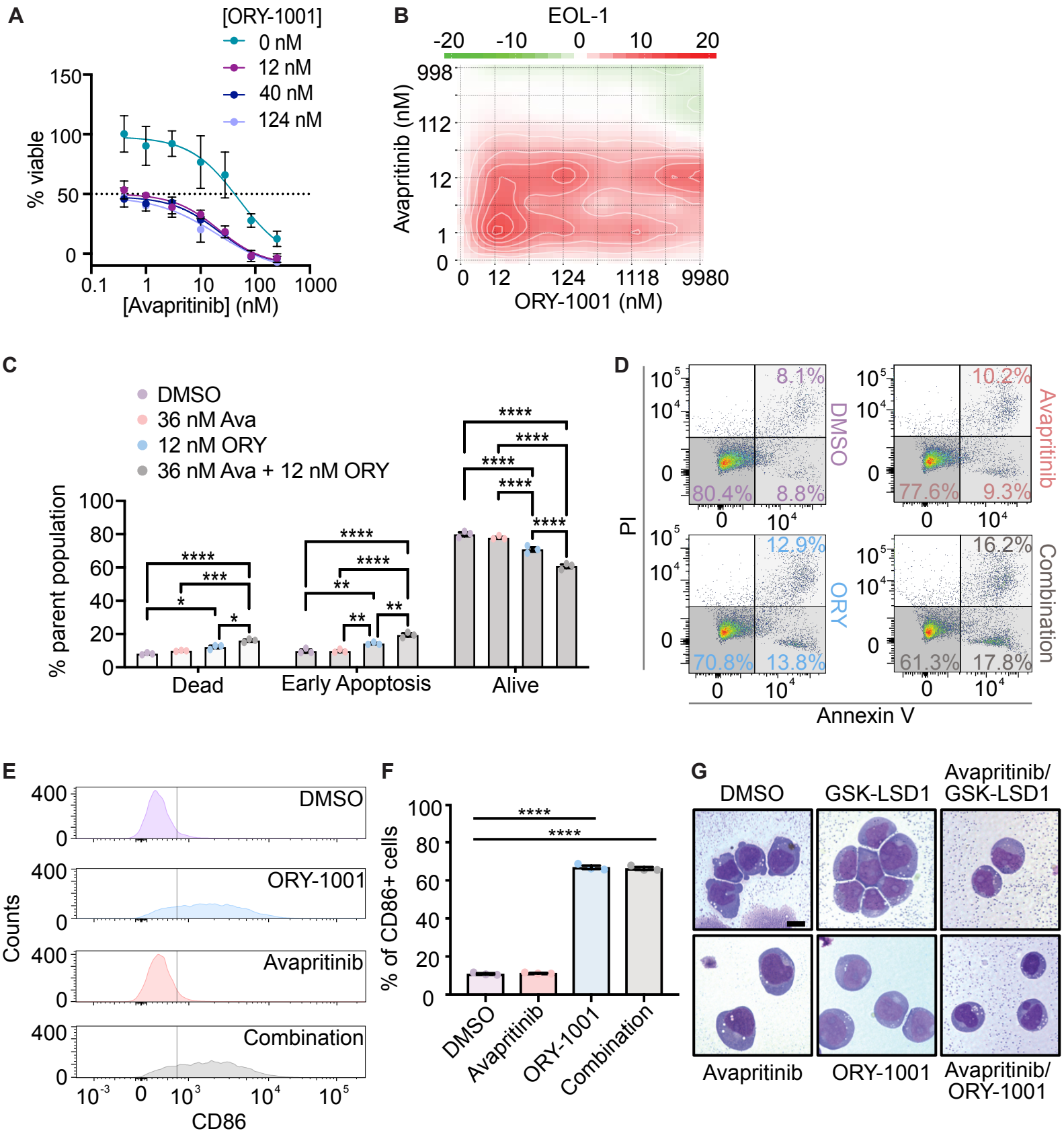

Supplemental Figure 2

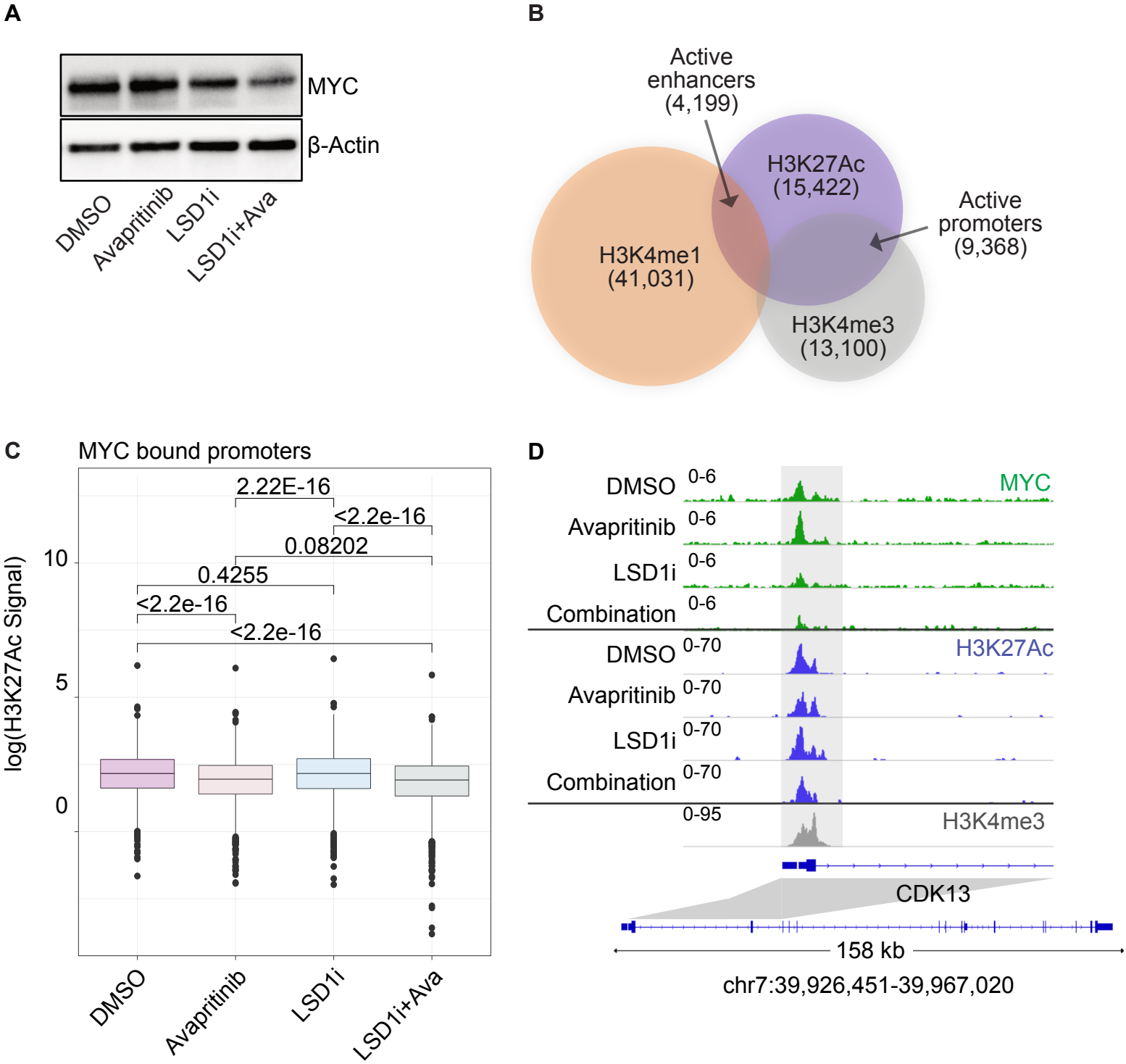

Supplementary Figure 3

A

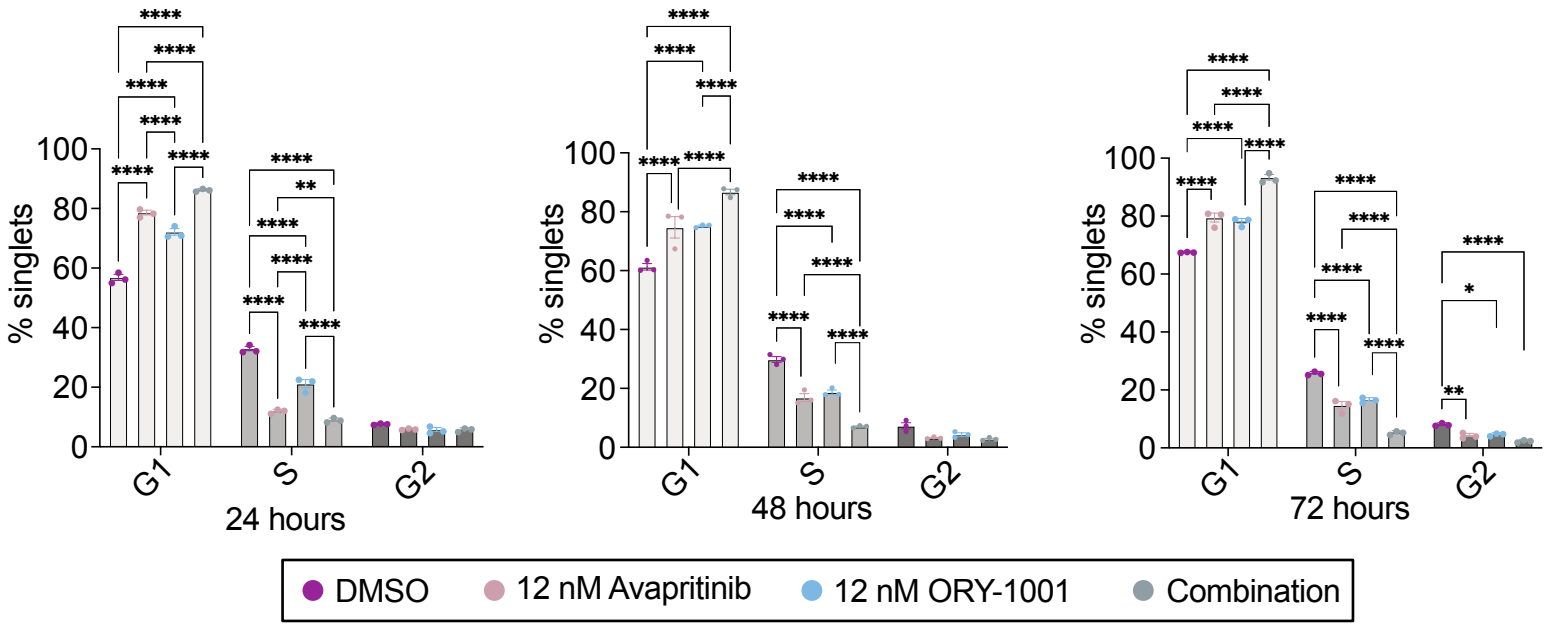

B

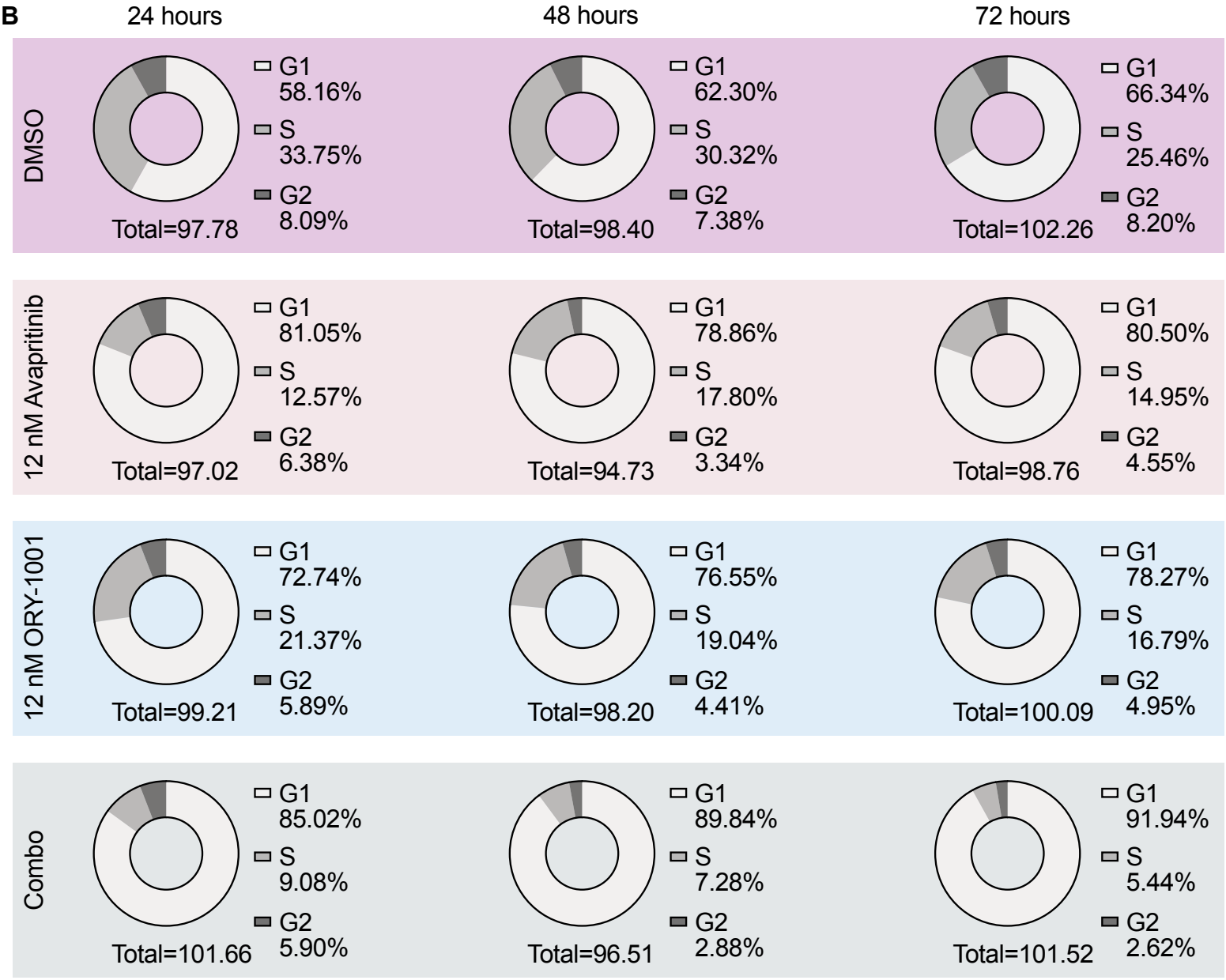

Supplementary Figure 4

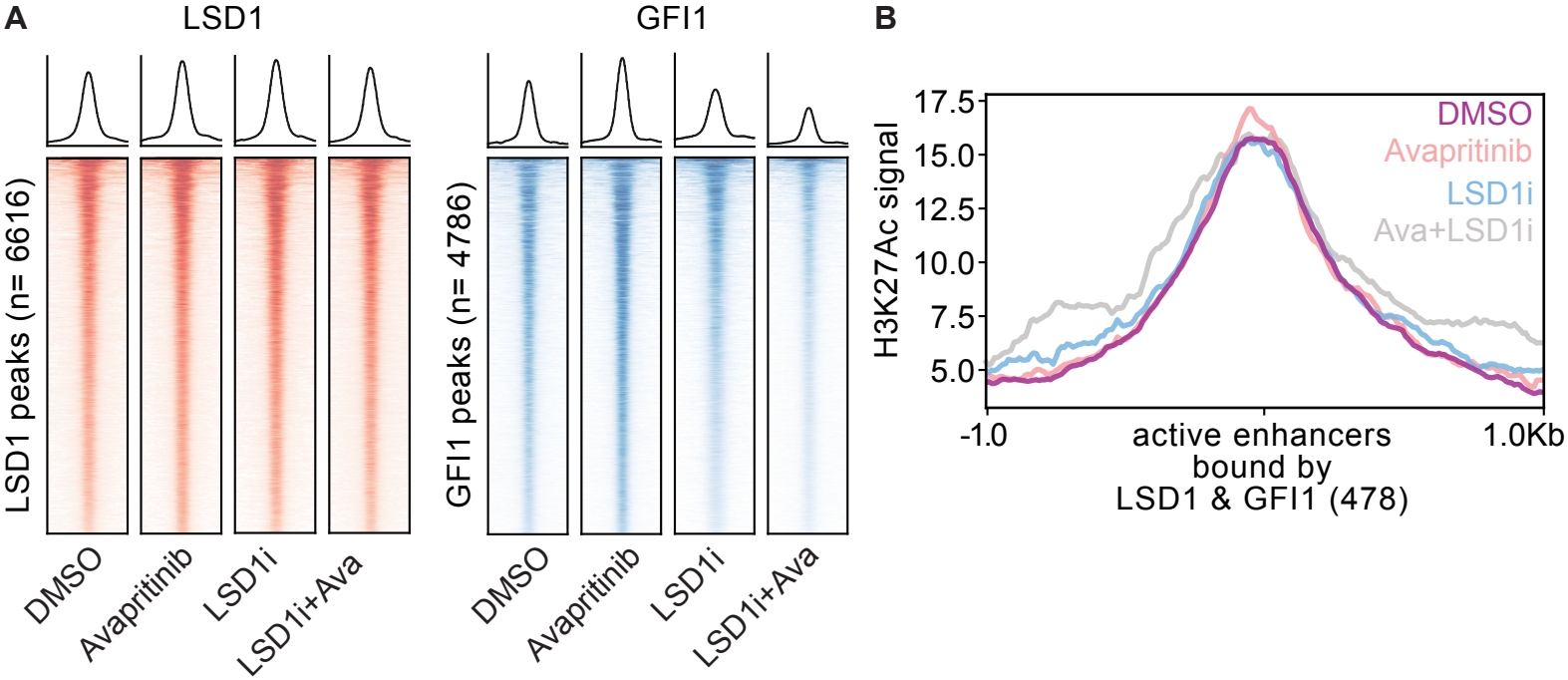

Supplementary Figure 5

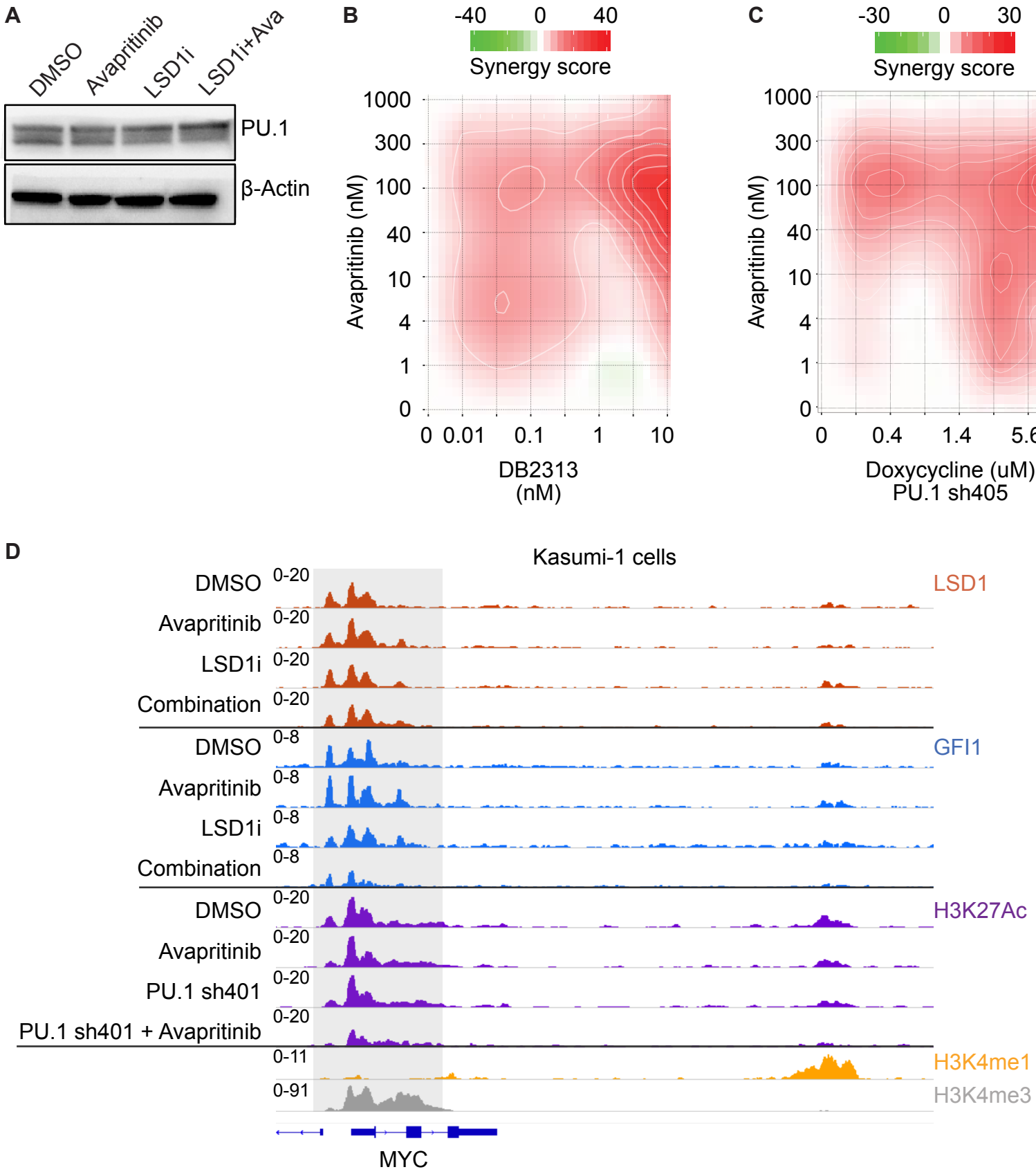

Supplementary Figure 6

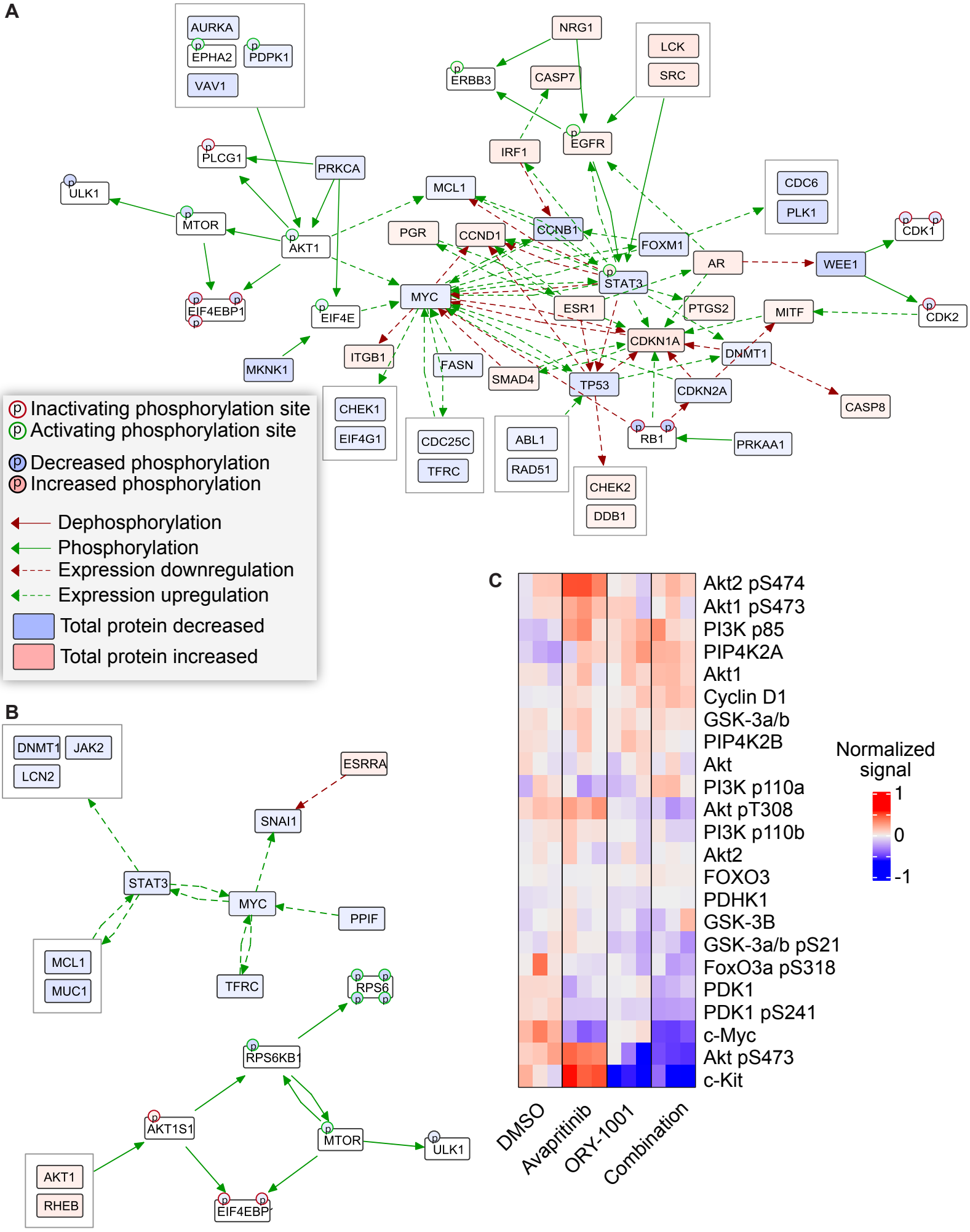

Supplementary Figure 7

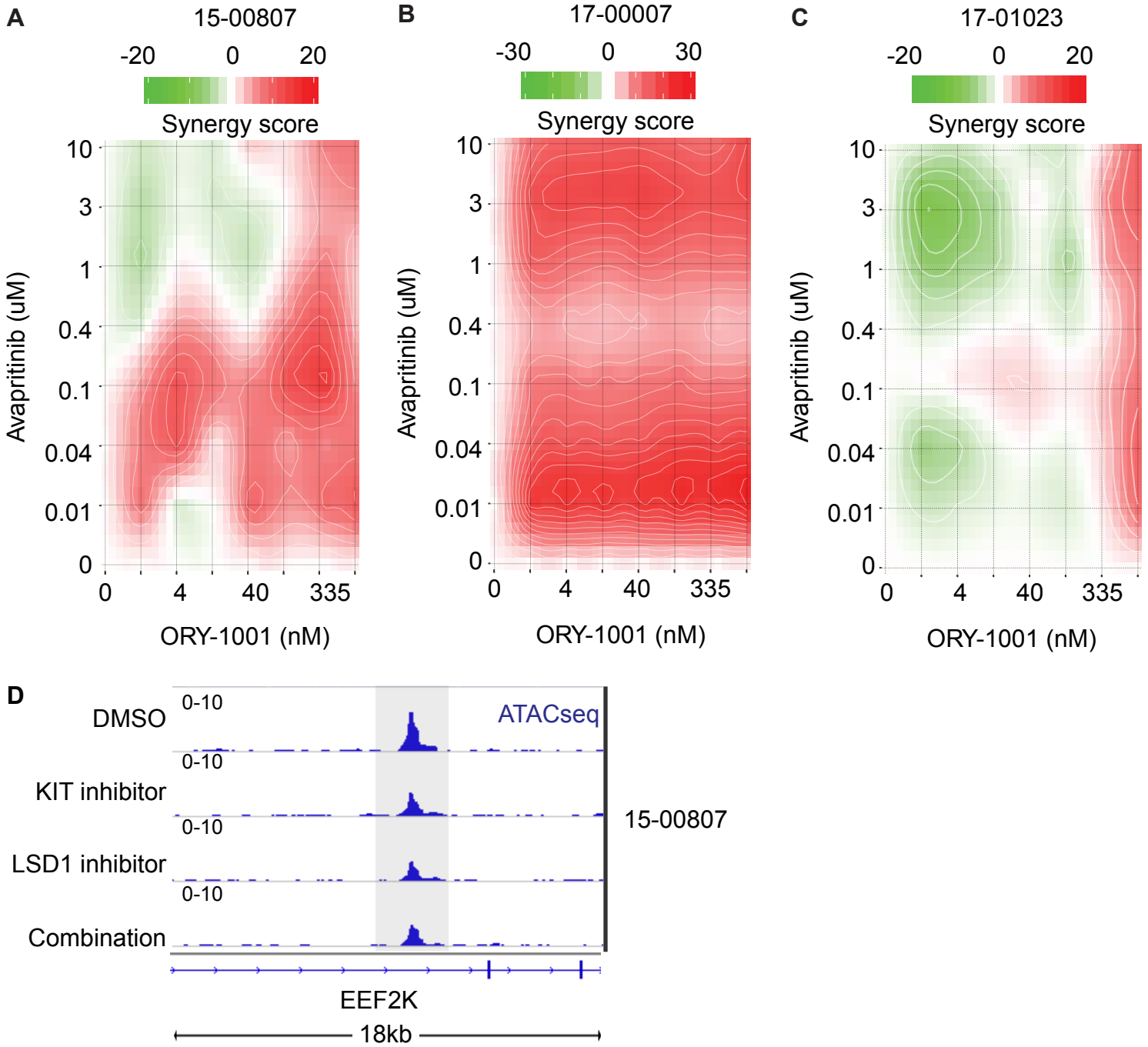
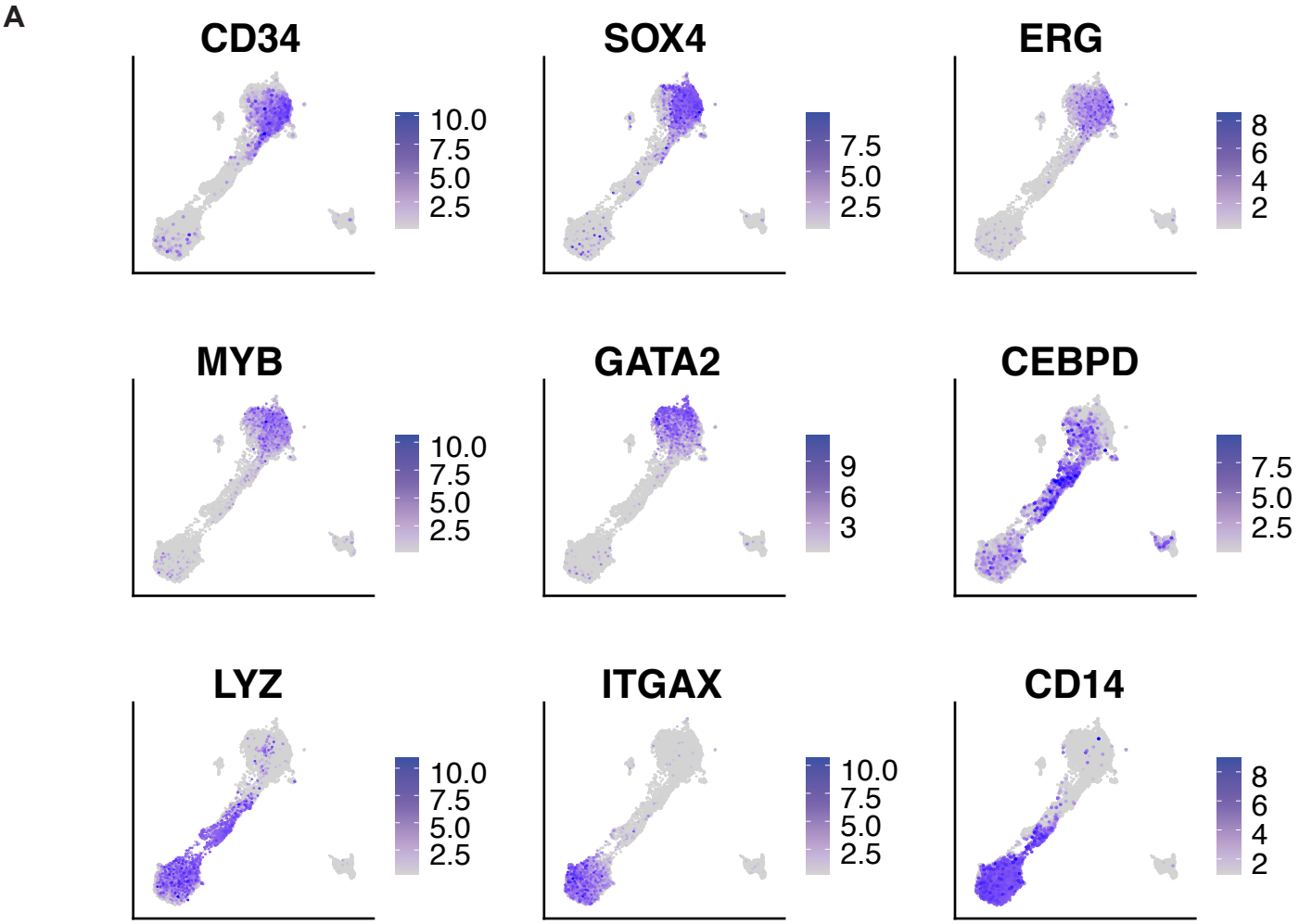
Supplementary Figure 8